Slow-moving landslide risk assessment combining Machine Learning and InSAR techniques

Novellino A.[a*], *Cesarano M.*[b], *Cappelletti P.*[b], *Di Martire D.*[b], *Di Napoli M.*[c], *Ramondini M.*[d], *Sowter A.*[e], *Calcaterra D.*[b]

[a] British Geological Survey, Environmental Science Centre, Keyworth, Nottingham, NG12 5GG, UK
[b] Department of Earth, Environment and Resources Sciences, Federico II University of Naples, Naples, 80138, Italy
[c] Department of Earth, Environmental and Life Sciences, University of Genoa, Genoa, 16132, Italy
[d] Department of Civil, Architectural and Environmental Engineering, Federico II University of Naples, Naples, 80125, Italy
[e] Terra Motion Limited, Ingenuity Centre, Nottingham, NG7 2TU, UK

[*] Corresponding author

Abstract

This paper describes a novel methodology where Machine Learning Algorithms (MLAs) have been used to assess the landslide risk for slow moving mass movements, processes whose intermittent activity makes challenging any risk analysis worldwide.

MLAs has been trained on datasets including Interferometric Synthetic Aperture Radar (InSAR) and additional remote sensing datasets such as aerial stereo photographs and LiDAR and tested in the Termini-Nerano landslides system (southern Apennines, Italy).

The availability of such a wealth of materials allows also an unprecedented spatio-temporal reconstruction of the volume and the kinematic of the landslides system through which we could generate and validate the hazard map.

Our analysis identifies fifteen slow-moving phenomena, traceable since 1955, whose total area amounts to 4.1×10^5 m^2 and volume to $\sim 1.4 \times 10^6$ m^3. InSAR results prove that seven out of the fifteen slow-moving landslides are currently active and characterized by seasonal velocity patterns. These new insights on the dynamic of the landslides system have been selected as the main independent variables to train three MLAs (Artificial Neural Network, Generalized Boosting Model and Maximum Entropy) and derive the landslide hazard for the area. Finally, official population and

buildings census data have been used to assess the landslide risk whose highest values are located in the crown area, south of Termini village, and nearby Nerano.

This new methodology provides a different landslide risk scenario compared to the existing official documents for the study area and overall new insights on how to develop landslide risk management strategies worldwide based on a better understanding of slope processes thanks to the latest satellite technologies available.

Keywords: landslides; InSAR; Machine Learning Algorithms; landslide hazard; landslide risk.

1. Introduction

Landslides are ubiquitous in any terrestrial environment with slopes, driven by tectonic, climatic and/or human activities (Froude and Petley, 2018). In particular, slow-moving landslides, which move downslope for months to decades at rates ranging from millimetres to several metres per year, provide an excellent opportunity to study landslide processes (Lacroix et al., 2020). Even if slow-moving landslides rarely claim lives, they still cause widespread destruction and if they rapidly accelerate result in casualties (Handwerger et al., 2019).

Slow-moving landslide events are recurring phenomena in southern Italy (e.g., Novellino et al., 2015; Di Martire et al., 2016; Pappalardo et al., 2018) due to its geological history and tectonic-geomorphological evolution which resulted in the occurrence of several formations identified as Structurally Complex Formations (SCFs; Esu, 1977), flysches or Broken Formations (Mutti et al., 2009). The term refers to geological units constituted by lithologically and structurally heterogeneous terrains with extra-formational blocks (D'Elia et al., 1998), associable to preorogenic and synorogenic turbidites of the Alps-Apennine system (Alvarez, 1991). The high heterogeneity and very poor mechanical properties of the SCFs represent one of the main factors contributing to the predisposition of slopes to landslide (Del Soldato et al., 2018). The latest Inventory of Landslide Phenomena in Italy report (IFFI) carried out by the Italian National Institute for Environmental Protection and Research

(ISPRA, 2018) evidences that slides, flows and composite phenomena (Hungr et al. 2014)). account for ~30% of the 620,808 mass movements inventoried in Italy. These three types of movements are typical of instabilities generated in SCFs (Fig. 1a), which have a huge impact on the Italian socio-economic system (Salvati et al., 2010) due to the shorter return periods (Fig. 1b) and higher spatial density (Fig. 1c) than landslides generated in other types of terrains.

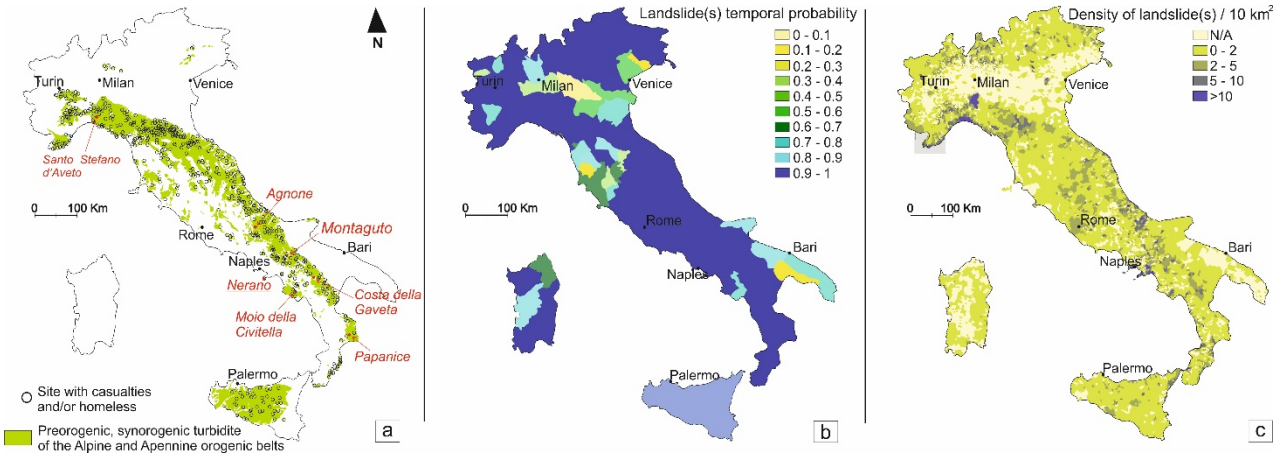

Fig. 1. *Spatial distribution of landslides resulting in casualties and/or homeless in Italy between 650-2008 (modified from Salvati et al., 2010) within SCFs-like outcropping units mapped following the 1:250,000 geological map of Italy (available at: http://www.isprambiente.gov.it/en/projects/soil-and-territory/the-geological-map-of-italy-1-250000-scale/default) with location of well-known landslides in SCFs from literature (a). Landslide temporal probability between 2018-2028 in Italy (b). Landslide density in Italy (c). Landslide data are available at: http://webmap.irpi.cnr.it/webmap_test/webmap.html*

The variability of material properties and landslide kinematics in SCFs, with a long state of activity at intermittent rates of displacement, makes any estimation of the corresponding risk challenging. To this respect, field-based monitoring systems (e.g., extensometers, crack meters, inclinometers, GNSS receivers) only provides spatially discontinuous, costly, labour intensive and time-consuming information. On the contrary, the use of remote sensing methods, like Interferometric Synthetic Aperture Radar (InSAR) represents a time-saving and cost-effective approach for understanding landslides kinematics (Novellino et al., 2017a), namely the hazard and deriving the corresponding risk. Landslide hazard is the likelihood of a potentially damaging landslide occurring within a given area with landslide risk being the spatio-temporal probability of the expected losses to life and damage to property, should a landslide occur (van Westen et al., 2008) and landslide risk maps (LRMs) represent essential tools for effective land use management and planning (Fell et al., 2008). Given the

high number of events, the challenge of assessing landslide risk related to slow-moving phenomena is particularly evident in Italy where this mandate, since 1998, belongs to the River Basin Authorities (recently merged in eight national Hydrographic Districts). River Basin Authorities have produced landslide hazards and risk maps which cover the whole Italian territory at scale ranging between 1:5,000 to 1:25,000. These maps represent official tools for land use and urban planning activities but are limited by common drawbacks: are usually produced from input datasets not regularly updated and mainly based on data-driven empirical methods which do not account for characteristics such as landslide velocity or the uncertainty in the maps themselves.

Despite various recent initiatives (Confuorto et al., 2017; Hu et al., 2020), the use of multidisciplinary approaches where InSAR has been deployed for a complete analysis of landslide kinematics and driving mechanisms is still limited and, consequently, the translation of these information in LRMs is even rarer so resulting in the absence of measures sufficient for landslide risk management/reduction.

The aim of this study is therefore to develop and validate a new methodology to assess landslide risk for slow-moving landslides based on Machine Learning Algorithms (MLAs). Recently, MLAs and in particular Ensemble Modelling (EM) has provided a solid contribution to minimize the uncertainty and improve the reliability of landslide mapping prediction by accounting for different data-driven methods together (Chen et al., 2017). To this, Ensemble methods have been proposed to combine the advantages of each stand-alone models and to mitigate the effects of their drawbacks (Thuiller et al., 2009).

In this work, we have trained three MLAs, Artificial Neural Network (ANN), Generalized Boosting Model (GBM) and Maximum Entropy (MaxEnt) with geological, geomorphometric and, for the first time, InSAR datasets to obtain a relative landslide hazard map. The latter has been then combined with data from the population and building environment to derive a relative risk map. MLAs methodologies have been recently applied in the literature to rapid landslides (Di Napoli et al., 2020) but, to our knowledge, not yet to slow ones.

MLAs have proven to outperform, especially at catchment and regional scale, heuristic and statistical models as they can address the nonlinear corrections between landslides and conditioning factors and can determine model parameters automatically (Huang et al., 2020). We tested our method for an area which has experienced rapid urban expansion first and tourism then: Termini-Nerano (southern Italy). Specifically to the area of study, our work has allowed to update the existing inventory map dated 2011 and compiled by the Southern Apennines Hydrographic District (SAHD, 2011a) and then improve the existing landslide risk map (SAHD, 2011b). More generally, our new methodology has already potential to be implemented at national and continental scale and, provided that the input data are available, easily applied worldwide.

The paper is organized as follows: a description of the geological-geomorphological setting of the Termini-Nerano site with a brief description of the landslide event history is provided in Section 2; the methodological approach developed for assessing the landslide risk is described in Section 3 along with the datasets used. The results are shown in Section 4 followed by the discussion and conclusions in Section 5 and 6, respectively, where we analyse why and how our approach can be extended elsewhere.

2. The Termini-Nerano landslides system

The studied area is located on the south-facing coast of the Sorrento Peninsula, southern Italy (Fig. 2) where the landslide system affects three villages, Termini, Nerano and Marina del Cantone. Geologically, the Termini-Nerano area belongs to the shallow-water carbonates succession of the Lattari-Picentini Unit, in the western sector of the Apennine Carbonate Platform (Vinci et al., 2017). According to ISPRA (2015), the outcropping rocks are composed of pre-orogenic Mesozoic carbonate sequence of the Radiolitidae limestone Formation (Upper Cretaceous; Iannace et al., 2011) topped by synorogenic terrigenous deposits of Miocene age including the Recommone Calcarenites Formation (Lower Miocene), the Termini Sandstones Formation (TSF - Miocene) and the Punta del Capo Breccias (Upper Miocene; D'Argenio et al., 2011). Quaternary deposits consist of slope debris,

derived from the limestone and sandstone bedrock, pyroclastic, and beach deposits. The latter cover the bedrock succession at limited spots, such as Marina del Cantone, but not at the Termini-Nerano valley. The Miocene TSF (200m thick) is divided into two members: the lowermost is the Nerano Member where the studied landslides developed. It consists of arkosic sandstones, interbedded with siltstone and mudstone levels, cropping out south of Termini. A gradual vertical and lateral transition leads to the Marciano Member, a thin-bedded arkosic turbiditic sandstone succession interbedded with marly levels. The tectonic features which most influence the local geomorphology are connected to a first compressional event with a NE-vergence, followed by an extensional one (ISPRA, 2015). The compressive phase created gentle folds in the TSF with the Upper Cretaceous carbonates thrusting over the TSF (Vitale et al., 2017) and determined the attitude of the Nerano Member to be converging towards the valley centre (Fig. 2).

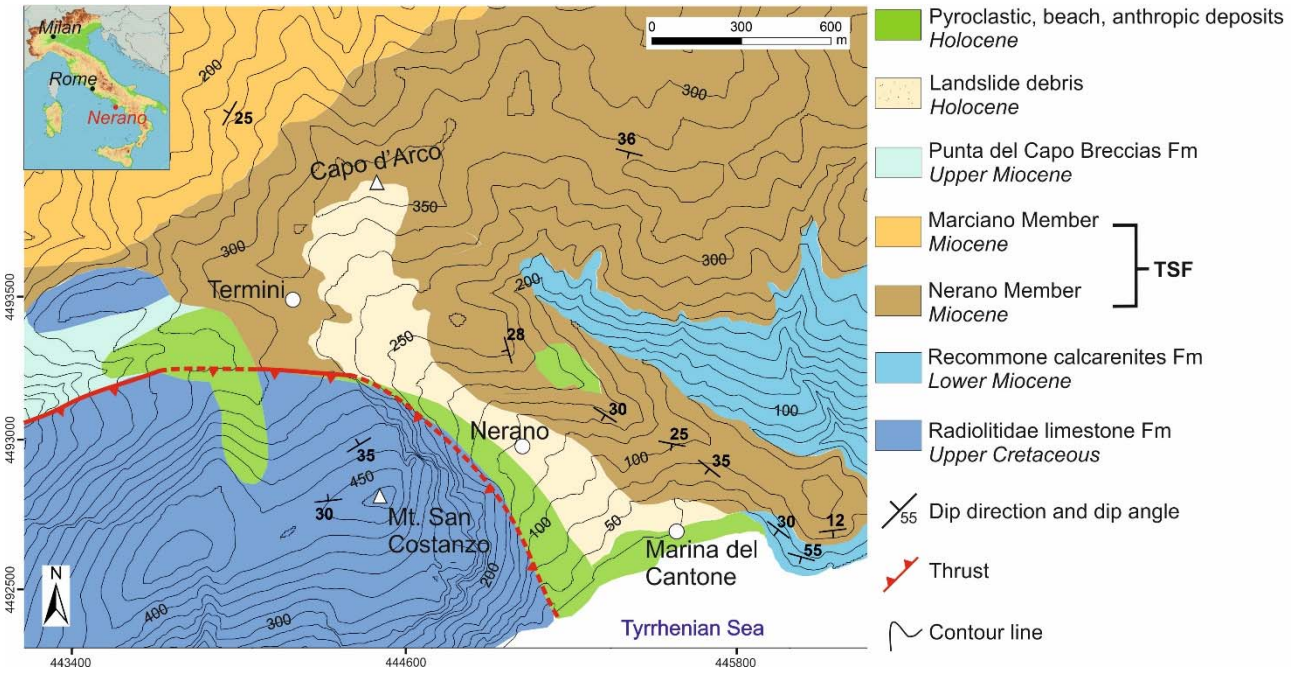

Fig. 2. *Geological map of the Termini-Nerano area. Coordinate system: WGS 1984, UTM Zone 33N.*

The mesoscopic scaly texture of the clayey intervals combined with the strong tectonic deformation and the presence of calcareous exotic blocks in the TSF, represent an important predisposing factor to slope instability in the area and a classical example of a SCF with geotechnical properties

149 intermediate between soils and rocks, strongly dependent on the scale of the mechanical
150 discontinuities.
151 According to historical chronicles, archive documents, local witnesses and data from the Italian
152 National Research Council (Canuti et al., 1992; de Riso et al., 2004), the valley has been affected by
153 several instability events in the recent past. The oldest phenomenon reported occurred in the 17th
154 century with successive reactivations recorded in 1910, 1939, in late December 1940 and early
155 January 1941. The latter involved a 2.1 $\times 10^5$ m^2 area and a 2×10^6 m^3 volume and destroyed the
156 Termini-Capo d'Arco road and some houses in Termini (Brugner and Valdinucci, 1973). The
157 following reactivation took place in Capo D'Arco hill, northeast of the village of Termini, on 19th of
158 February 1963 and lasted seven days (Cotecchia & Melidoro, 1966). The event was triggered after
159 101 mm of cumulative rainfall in the previous 24 hours and 217.4 mm in the previous 19 days,
160 corresponding to almost 20% of the 1963 annual rainfall budget. Landslide velocity ranged from 3
161 m/h to 27 m/h (Cotecchia and Melidoro, 1966); the movement started as a rotational slide and then
162 developed as a flow that struck the villages of Nerano and Marina del Cantone, ~900 m downslope,
163 before reaching the Tyrrhenian Sea. Seismic refraction studies in the aftermath of the event localized
164 the main rupture surface at ~25 m of depth (Cotecchia & Melidoro, 1966) and reported a total length
165 of the landslide body of ~1,900 m with an area of 1 $\times 10^5$ m^2 and a volume of 1×10^6 m^3. The current
166 landslide inventory map (SAHD, 2011a) identifies 20 different sub-movements (five falls, three
167 rotational slides and twelve complexes) within the Termini-Nerano valley, covering a total area of 4
168 $\times 10^5$ m^2 (Fig. 3a). The SAHD inventory is based on a combination of aerial photography and Digital
169 Terrain Model (DTM) interpretation complemented by field surveys. The inventory is then combined
170 with geomorphological predisposing factors to derive the susceptibility and finally is overlaid to
171 vulnerability and exposure information to empirically asses the risk levels following a matrix-based
172 heuristic approach (Fig. 3b).

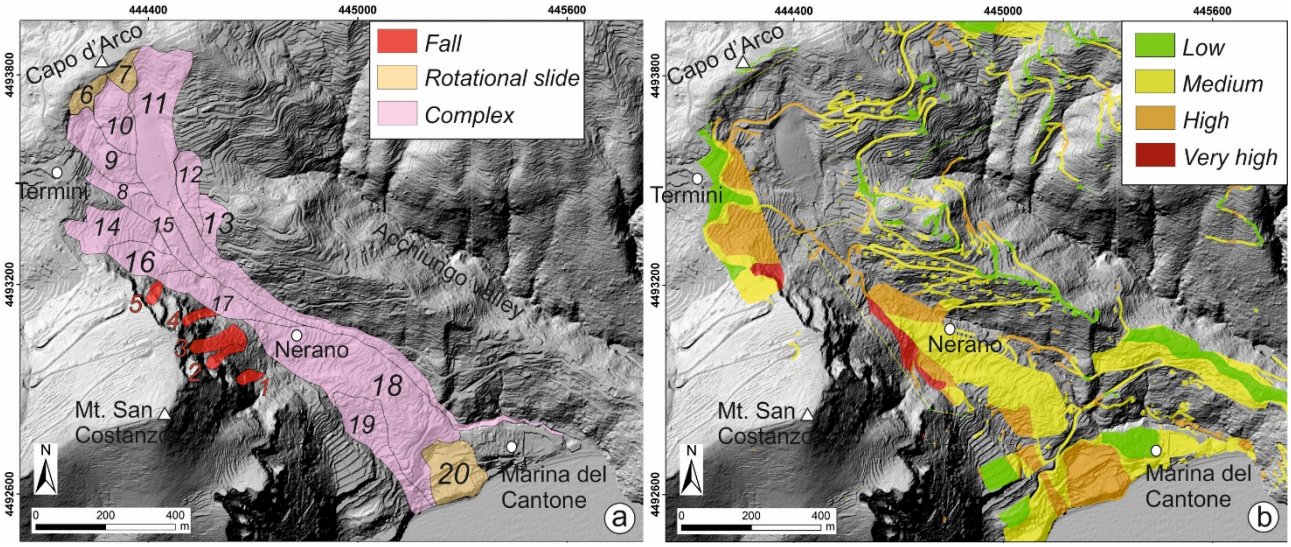

Fig. 3. Landslide inventory map (SAHD, 2011a) where each number refers to a single landslide classified according to the type of movement (a). LRM (SAHD, 2011b) that shows the level of risk only where infrastructure are present (b). The two maps are overlapped onto shaded relief DTM. Coordinate system: WGS 1984, UTM Zone 33N.

The LRM is therefore generated with a method based on expert opinion which, inevitably, cannot account for the many uncertainties associated with the landslide processes.

3. Materials and methods

The multidisciplinary approach of the work has been designed to define the relative landslide risk (R) limited to the slow-moving phenomena (Figure 4). Different investigations have been performed to retrieve the characteristics of the landslides needed for assessing and validating R.

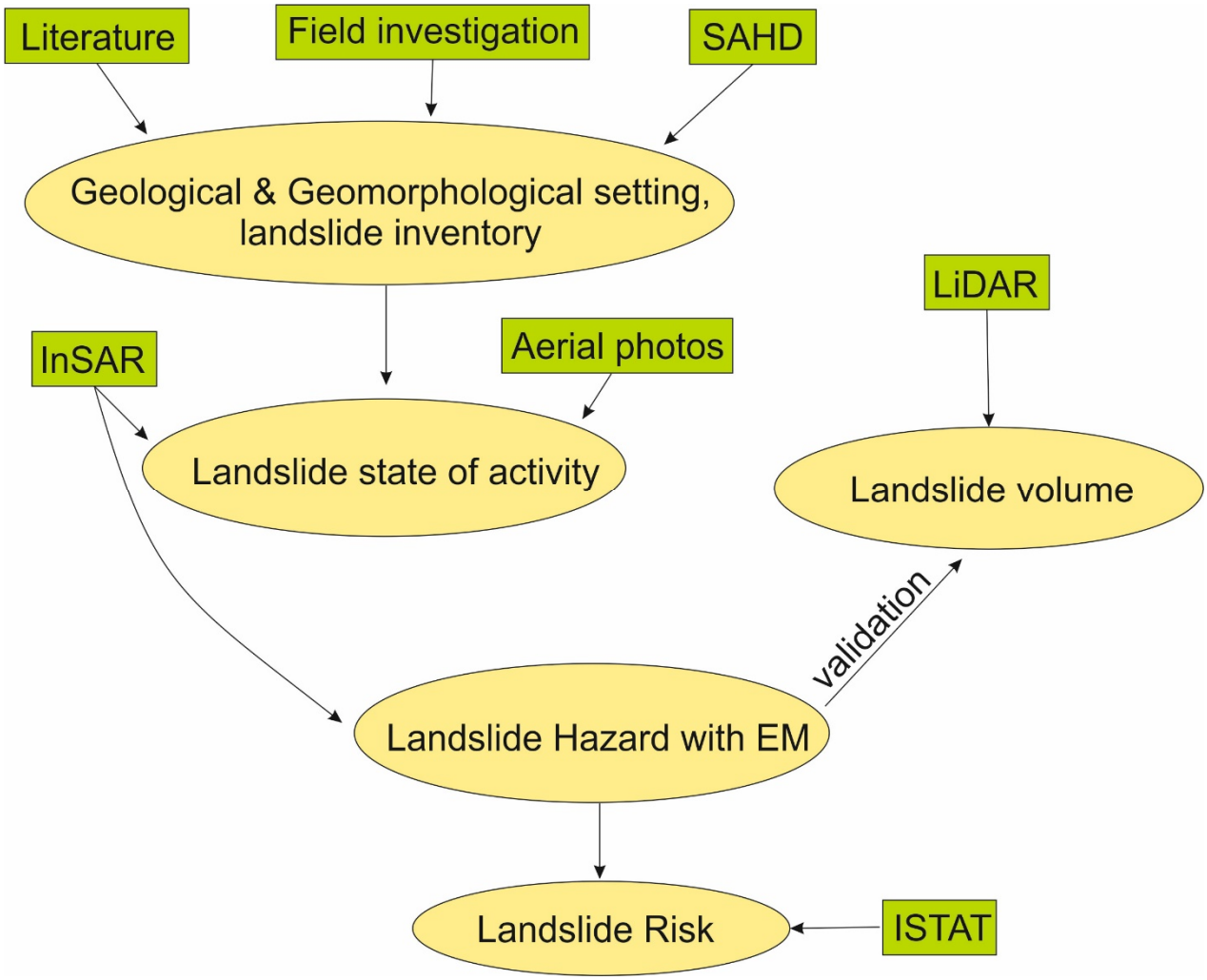

Fig. 4. *Workflow of the approach adopted in this work. Techniques and input data are in green, outputs in cream. Inputs data include the landslide inventory and geomorphological maps from the Southern Apennines Hydrographic District (SAHD), ground deformation displacement from Interferometric Synthetic Aperture Radar (InSAR), hazard maps from the Ensemble Modelling (EM) and exposure and vulnerability data from the Italian National Institute of Statistics (ISTAT).*

The geological and geomorphological information of the valley have been derived from field surveys conducted between 2012 and 2013 and then integrated with sub-surface data acquired though five boreholes drilled in landslides 11 and 18 where, successively, three inclinometers and two open stand-pipe casings have been installed, recording data from different sectors of the valley (Fig. 5). These investigations provided information on the type of materials involved in the instability and its

197 kinematics, constrained the volumes associated to the active part of the landslide and validated the
198 InSAR results.
199 The remote sensing dataset allowed the understanding of the state of activity of the movements, the
200 interaction between the instability zones within the valley and the estimation of the landslide volumes.
201 Remote sensed data include aerial stereo photographs, LiDAR DTM and InSAR velocities maps.
202 Aerial stereo photographs for the 1955-2011 time span were obtained from the Italian Military
203 Geographic Institute and the Agency of Agriculture, Food and Forestry of the Campania Region, the
204 acquisitions were taken at flying heights ranging from 2,700 m to 6,200 m with a scale ranging
205 between 1:10,000 and 1:41,000. The DTM, acquired from airborne 2012 LiDAR data, with a
206 resolution of 1 m and root mean square error of ~0.15 m (http://sit.cittametropolitana.na.it/lidar.html),
207 has been used to assess the original volume associated to each landslide. InSAR results have been
208 generated from 35 ascending and 35 descending COSMO-SkyMed (CSK) X-band images acquired
209 in the 20/10/2011 – 19/4/2014 and 20/2/2012 – 23/12/2013 interval, respectively. The two geometries
210 have been processed at 3m×3m resolution by means of the Persistent Scatterer Pair technique (PSP;
211 Costantini et al., 2014) as part of the third phase of the Not-ordinary Plan of Environmental Remote
212 Sensing project (Piano Straordinario di Telerilevamento Ambientale – PST-A), a nationwide
213 monitoring plan run by the Italian Ministry of Environment and Protection of Land and Sea in
214 cooperation with the Italian Space Agency (Costantini et al., 2017; Di Martire et al., 2017).
215 The EM has been trained to produce the landslide hazard (H) via three MLAs (ANN, GBM and
216 MaxEnt) well-known for their good performance (Elith et al., 2006). ANN refers to a large group of
217 models that are inspired by biological neural networks to process information. These networks are
218 typically structured in layers with an input layer containing the environmental variables used to train
219 the model, several hidden layers in which the function applies weights to the inputs and directs them
220 through an activation function as the output (Dou et al., 2015). GBM is a ML technique for regression
221 and classification models. GBM repeatedly perform many decision trees to enhance model precision.
222 For each new tree in the model, a random subset of all the data is selected using the boosting method,

223 which iteratively aims to reduce the errors of the previous one (Kim et al., 2018). MaxEnt is a
224 "presence-only" spatial distribution method. It makes use of occurrence data and a large number of
225 points throughout the study area, known as background points. MaxEnt calculates the ratio between
226 two probability densities (occurrence and background points), which gives the relative
227 "environmental suitability" for the presence of an event for each location in the study area (Sepe et
228 al., 2019). The MLAs use predisposing factors determined and assessed from the geological,
229 geomorphological and kinematic characteristics of the instabilities which do not show collinearity
230 according to the Variance Inflation Factor (VIF) calculation (Arabameri et al., 2019). To perform and
231 assess models achieved with various MLAs, the K-fold Cross-Validation (K-CV) approach was used.
232 The latter splits a random part of the input population (~80%) for calibration while the remaining
233 (~20%) is used for testing the prediction of the model; the entire approach is then replicated several
234 times for each of the three models and the average predictive accuracy is finally reported through the
235 Area Under the Receiver Operating Characteristic (AUROC) curve and True Skill Statistic (TSS)
236 (Araujo et al., 2005). Afterwards, the three MLAs were ensembled and H was evaluated by
237 considering the median values of the spatial probability of landslide occurrence from the three
238 models. The short temporal interval of the InSAR time series, 3 years, despite provides a constraing
239 on the landslides state of activity do not provide sufficient records to assess the return periods of the
240 landslide which tend to occur in the range of tens of years in this area (see Section 2). So the H defined
241 in this paper is a relative hazard which does not account for the probability of landslides occurrence
242 within a given period of time, a solution already adopted whenever the knowledge of landslide
243 mechanisms is limited (Andrejev et al., 2017).
244 H has been integrated with information on local population and buildings to generate R which,
245 similarly to H, it refers to a relative risk. Spatially, the R can be conceptually represented as a non-
246 homogeneous Poisson process (NHPP) similarly to what has been done in Bartolini et al. (2013) when
247 simulating different eruptive scenarios:

248 $$R = 1 - \exp\big((H + V + E) * -1\big) \quad (1)$$

249 Where V is the degree of damage (namely the vulnerability) of a specific element-at-risk (E) inside
250 the area. H, V and E represent variables associated to the landslide that can change in time following
251 a non-homogeneous Poisson process with an exponential distribution. The probability density
252 function for V and E have been calculated over the territorial units defined by the Italian National
253 Institute of Statistics in 2011 (ISTAT, 2011) for the area of study.
254
255
256 **4. Results**
257 *4.1 Geological-geomorphological investigations*
258 Landslide events have intensively reshaped the superficial deposits of the Termini-Nerano valley
259 where the intensive urban development, especially between 1919 and 1990 according to ISTAT
260 (2011), is now partially covering geomorphological signatures of instabilities.The morphoevolution
261 of the valley occurs prevailingly through slides and flows and secondarily by rockfalls and surface
262 runoff through gullies (Fig. 5).

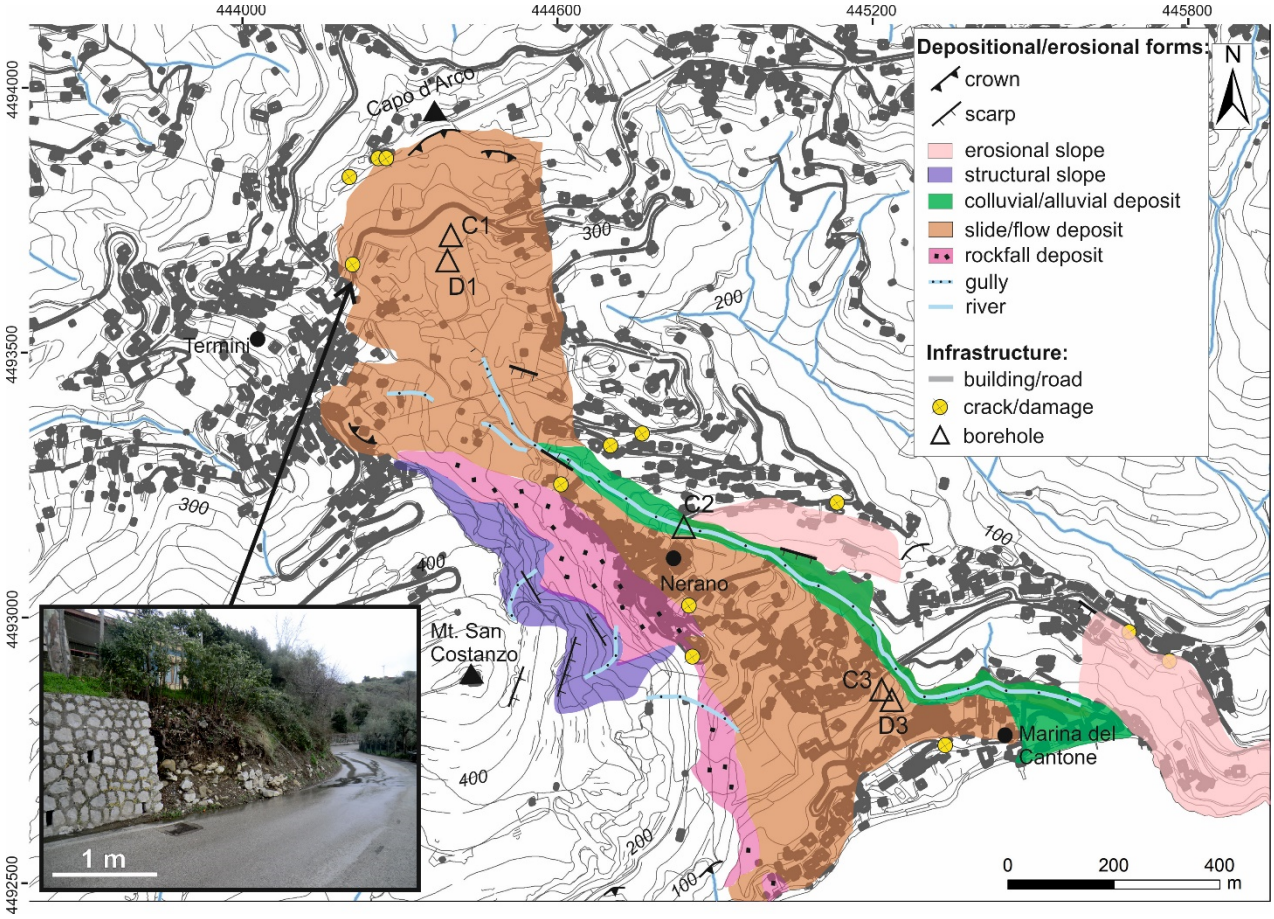

Fig. 5. *Geomorphological map of the Termini-Nerano valley where slope and superficial deposits have been classified according to the dominant morphogenesis. Coordinate system: WGS 1984, UTM Zone 33N (modified from SAHD, 2011c)*

The main scarp is associated to a ~15 m high crown area and is located in the Capo d'Arco area, on a 20º slope. Downslope, landslide flow and slide deposits from lateral lobes converge and fill the structurally-controlled NW-SE valley. Despite the anthropogenic disturbance, which has confined gullies on the eastern side of the valley, scarps in the order of some meters are still preserved in the landslide deposits within the catchment area. Gullies transport colluvial and alluvial deposits along a NW-SE direction which take a 90º bend downslope, just north of Marina del Cantone, where have been removed by human intervention to allocate space for leisure activities.On the western side of the valley, the mass movement deposits are topped by coarse-grained rockfall material from Mt. San Costanzo but are also embedded in the flow and slide deposits (Fig. 5).

The lithology of landslides 11 and 18 and its relationship with the bedrock was determined from drillcores (see Figure 3). The superficial units are mainly characterized by alternating beds of shales,

279 silts, sandstones and, in the transport and accumulation zones, calcarenitic-sandstones from the marly-
280 calcareous olistoliths of TSF (Fig. 6). The component of clay minerals, determined from laboratory
281 grain-size analyses, increases from 10 % wt. in C1 to 20 % wt. in C2 and 30 % wt. in C3 (Cesarano
282 et al., 2018).

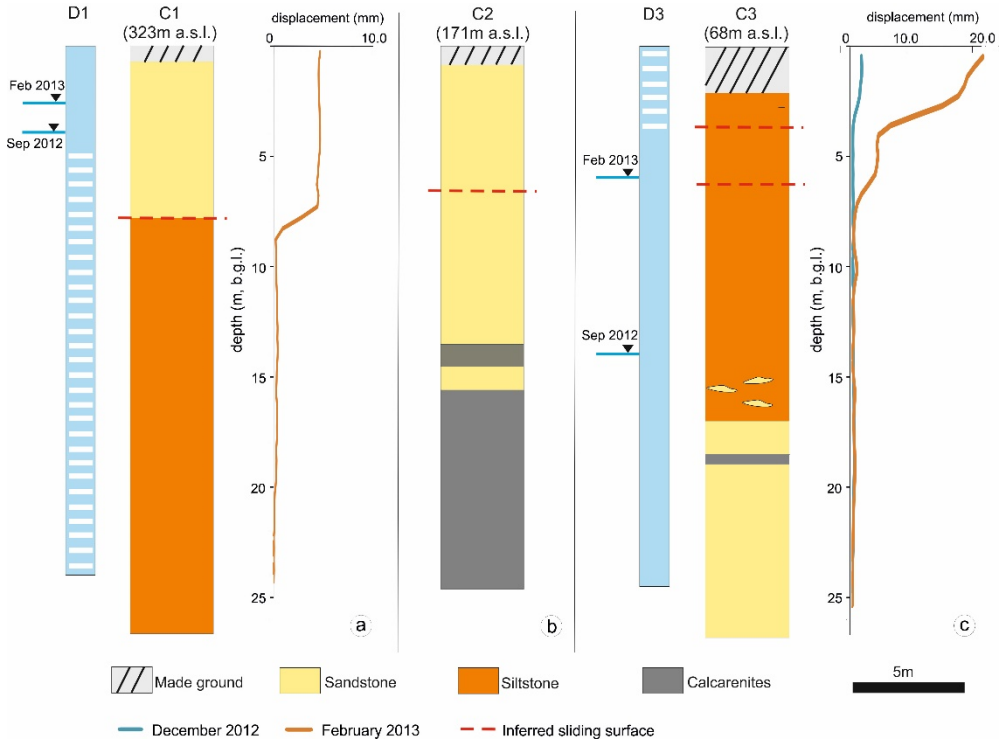

283

284 ***Fig. 6.*** *Sketch showing the stratigraphic logs of the units investigated. Piezometers installed are represented in blue with*
285 *white stripes indicating the screened section of the borehole. Inclinometer's zero reading: September 2012. Location of*
286 *the boreholes is provided in Figure 5.*
287

288 The shallower layers of superficial material are composed of poorly cemented sandstone or siltstone
289 levels with different degree of weathering and heterogeneity with depth, so confirming the presence
290 of overlapping mass movement deposits above the bedrock, the latter only found down to 20 m in C3
291 (Fig. 6). We have indeed interpreted the calcarenites levels in C2 as one of the exotic block embedded
292 within the TSF, being the Recommone Calcarenites Formation at ~100 m depth in this location.
293 Inclinometric data show a single slip surface at around 8 m depth in the upper part of the slope (C1)
294 with displacements of ~5 mm, and two slip surfaces in C3, at depth of 4 m and 6 m, with
295 displacements decreasing downwards and an overall disarranged structure down to ~20 m. No reliable
296 information could be reported from C2 as the aluminum casing broke at ~6 m b.g.l. soon after its

297 installation, suggesting at least one slip surface at such depth.These differences in the borehole
298 lithology and the measured inclinometric-material response play an important role in understanding
299 the kinematics of landslide 11 which is characterized by plastic deformation in the head area with a
300 motion similar to a slide which becomes a creep downhill where the clay fraction increases and the
301 failure surface is not so clear anymore.
302 Groundwater levels, measured from September 2012 to February 2013, suggest the occurrence of an
303 unconfined shallow aquifer located in the fractured mass above the slip surface which has different
304 characteristics in the crown and the toe area given the different response in groundwater rise (~ 1 m
305 in D1 and ~3 m in D3) for the 932 mm of rainfall occurred over this time interval.
306
307 *4.2 Aerial photography stereoscopic analysis*
308 The oldest aerial photos available, dating back to 1955, show sparse vegetation and extensive
309 outcrops of the TSF. The four main lobes belong to the 1941 landslides east of Termini that had
310 developed into a flow which had reached the village of Nerano and spread as soon as it reached the
311 Marina del Cantone village (Fig. 7a). The three main lobes correspond to the crown sectors of
312 landslides 9, 10, 11, 14 and 15 of the SAHD landslide inventory map (see Figure 3a). The 1974 aerial
313 photograph highlights remedial works carried out by the Public Works Department of Naples
314 following the 1963 landslides which led to the construction of retaining walls and drain trenches
315 connected to a drainage basin downslope (Fig. 7b). The imagery shows that the 1963 event developed
316 in the eastern sector of the Capo d'Arco hill, within the 1941 deposits, had an aerial extension ~30%
317 smaller than the previous event and was diverted almost at a right angle nearby the Marina del
318 Cantone village possibly by the 1941 toe zone, which might have confined the flow towards the
319 eastern side of the valley. The following bioengineering interventions allowed a pine forest to develop
320 on the surface of the 1963 landslide body, which matured in the following years, as evident from the
321 1990 frames (Fig. 7c). From 1990 onward, the intense urbanization of the area erased any
322 geomorphological evidence of the older landslides with vegetation wiped out by fall and topple

deposits generated from the eastern side of Mt. San Costanzo, sometime between the 70s and the 80s. In 2011, the intense urbanization of the area erased any geomorphological evidence of the older landslides (Fig. 7d).

The 1941 and 1963 event geometries control the following development of any smaller landslides between Capo d'Arco and Nerano that remobilise material from the past landslides. However, their slow velocity and dimensions do not provide scars identifiable in the stereo-photos but still observable on the field, such as the damage associated to landslides 6 and 7 and representing the retrogressive evolution of the landslides system (see Figure 5).

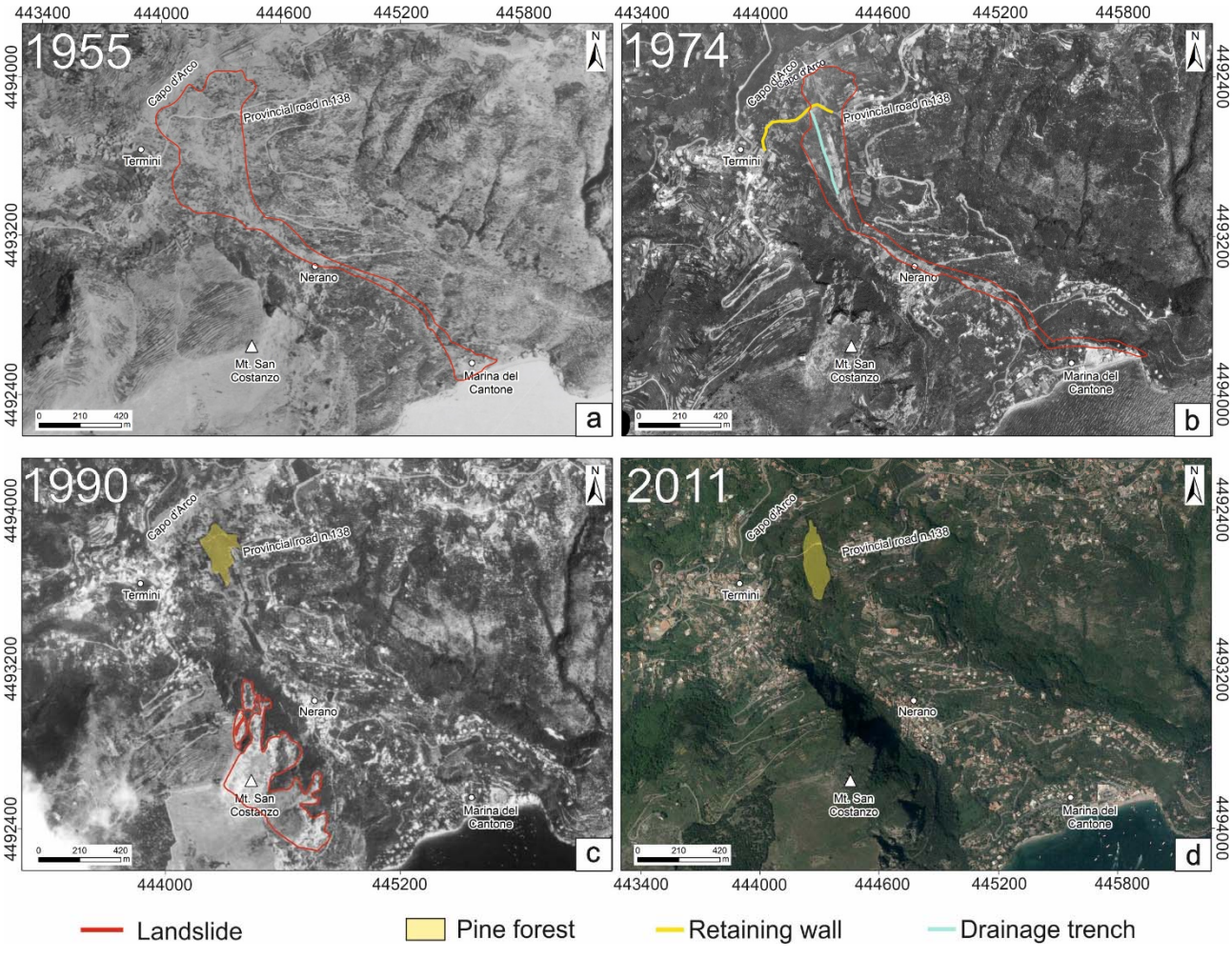

Fig. 7. *Inventory of the active landslides within the Termini-Nerano catchment from aerial stereo-photos: 1955 (a), 1974 (b), 1990 (c), 2011 (d). Coordinate system: WGS 1984, UTM Zone 33N.*

4.3 LiDAR analysis

The 2012 DTM has been used to reconstruct the pre-landslides (original) topography, retrieve the vertical differences between the current and original topography and then assess the volumes. The original topography has been defined by using as reference surface the topography from un-failed portions of the slopes. The reconstruction is based on three assumptions: the unslided wallslopes represent the original geomorphology of the area had the landslides not occurred (i), the sediment transport process, from sediment detachment to its depositions only occurs within this catchment (ii) and that human reprofiling (e.g., terracing, embankments) of the slope has had a limited impact on the elevations despite the wide urbanisation of the valley (iii).

The reconstruction has considered linear, exponential or logarithmic functions to perform a 1D fitting for profiles along and across the valley, similarly to what has been done in Chang et al. (2018). Of the three regression models, the one with the highest coefficient of determination (R^2) with the topographic profile has then been selected. A total of 41 profiles in the TSF parallel and orthogonal to the landslides have been considered (Fig. 8a):

- Five profiles parallel to the direction of motion of the landslide bodies, to represent the original topography along the main direction of the valley. These profiles have been derived from the regression of five profiles located outside the Termini-Nerano valley, in the northern facing slope of the Sorrento Peninsula (Fig. 8b). These sections have been chosen as they are largely unaffected by tectonic processes, human activities (terracing, re-profiling) and previous mass movements and have a similar elevation range to the Termini-Nerano valley. The best model retrieved from the five profiles outside the landslides has then been used to retrieve the pre-landslide longitudinal profiles along four profiles within the Termini-Nerano valley.

362 • Twenty-seven profiles transverse to the landslide bodies, to represent the original topography
363 across the main landslides pathways. In this case the west and east side of the Termini-Nerano
364 valley that are not part of the landslide have been fitted by the models independently (Fig. 8c).
365 Again, the transverse profiles were reconstructed by selecting the regression with the highest
366 R^2.
367
368 An envelope surface has been subsequently interpolated from the 32 profiles by using Inverse
369 Distance Weighting (IDW) method. The average R^2 value of 0.83 from the best fitting models along
370 the profiles supports the idea that, especially in the narrow parts of the valley with steeper surfaces,
371 the envelope surface can be considered an optimal way to reconstruct original topography.
372 Compared to the actual morphology, the envelope surface reveals a more rugged topography in the
373 crown area and a gentler slope at the bottom of the valley (<10° vs 20/30°). The
374 depletion/accumulation map could finally be retrieved from the vertical difference in the elevations
375 between the 2012 topography and the reconstructed topography (Fig. 8d).
376 Positive differences mean that the 2012 topography is above the original topography (i.e.
377 accumulation areas) while negative differences indicate that the 2012 topography is below the original
378 topography (i.e. depleted areas) as a result of the mass movements.

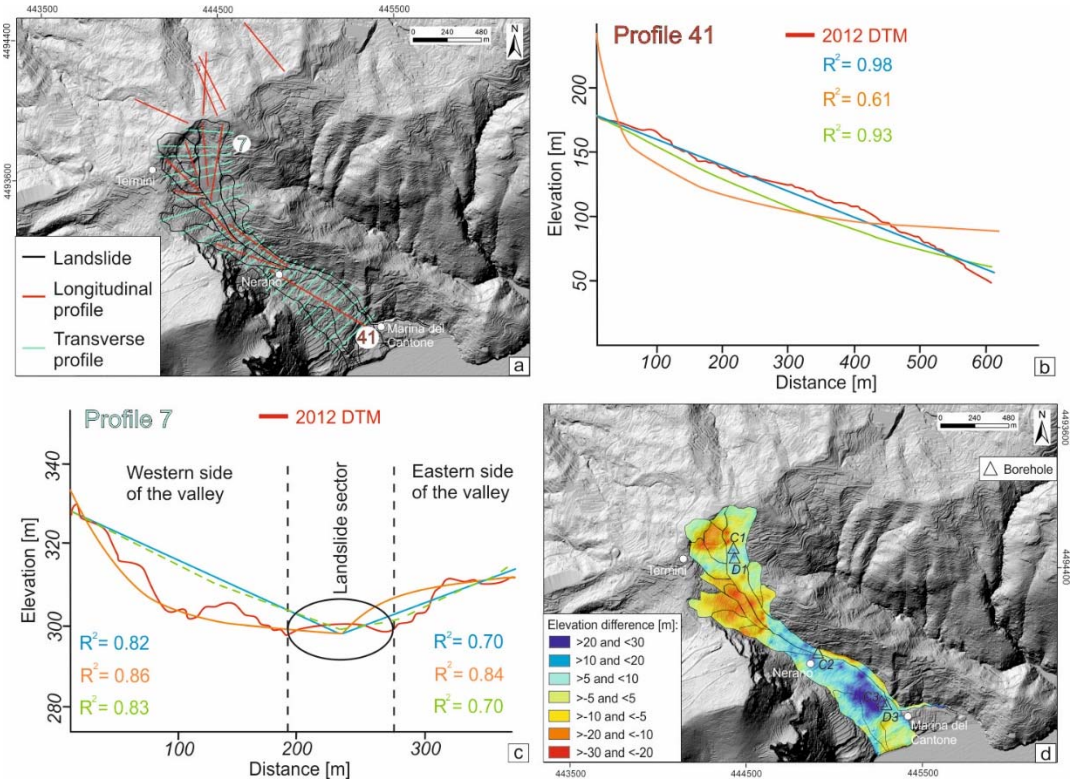

Fig. 8. *Location of the longitudinal and transverse profiles overlapped onto the hillshade map of the study area obtained from the LiDAR DTM (a). Example of the regression model for the longitudinal profile number 41 (b) and the transverse profile number 7 (c) where blue, orange and green colour refer to the linear, logarithmic and exponential fitting, respectively. Elevation difference between the 2012 DTM elevation and the reconstructed topography where positive values indicate accumulation areas and negative values indicate depleted areas (d).*

DTMs difference highlights two depletion areas, one spreads across the crown sectors of landslide 9, 10 and 11 and the other one where the mass deposits direction of flow converges in the narrow valley between Termini and Nerano (landslide 15 and 17), in this part elevation difference is -27 m. The accumulation area is instead located southward, between Nerano and Marina del Cantone, where the 2012 topography is 31 m higher than the reconstructed one. Vertical differences are usually 10 m lower than slip surfaces retrieved from the inclinometers, thus supporting the idea that the current moving landslides just involve the superficial deposits of the whole landslide mass.

By taking into account the area, vertical differences have been converted to volumes for each landslide. The volume differences prove that landslides 17, 18, 19 and 20 represent net accumulation areas while all the other landslides have a net mass loss. The spatial extension of landslide 11, from the crown to the toe, inevitably encompasses multiple areas of depletion and accumulation.

The whole displaced mass amounts to ~1.484×10^6 m^3, (Table 1).

Table 1*. Area, average elevation difference and volume gain/loss for each rotational and complex landslide in the Termini-Nerano valley.*

Landslide ID	area [m^2]	net volume difference [m^3]
6	11,931	-32,620
7	6,214	-38,181
8	7,637	-90,562
9	21,387	-101,827
10	17,932	-235,681
11	100,284	-89,503
12	11,975	-19,299
13	8,093	-55,820
14	25,427	-332,216
15	14,780	-279,220
16	14,768	-201,408
17	22,603	7,974
18	95,448	1,245,974
19	25,471	234,569
20	24,003	4,298
Total	*407,954*	*16,477*

Because historically small landslides within the Termini-Nerano valley develop within the older deposits, is likely that reactivations will be fed by materials located southeast of Nerano, especially at the steep eastern edge of landslide 18 where a net accumulation sector has formed. Considering the positions of the sliding surfaces measured at C1, C2 and C3 within landslide 11 and 18, we can estimate that a volume of at least ~$0.67 \pm 0.03 \times 10^6$ m^3 is currently active.

4.4 InSAR analysis

InSAR measurements have been used to characterize the slope kinematics. By taking into account the standard deviation (σ) of the LOS (Line of Sight) velocities such as in Aslan et al. (2020), the stable target threshold has been set to ±1.5 mm/yr, ~2 times σ. The results reveal the presence of many areas still affected by surface displacements along the basin and related to active slope instability phenomena with the presence of vegetation that hinders the density of radar targets.

CSK results (Figs. 9) for the period 2011-2014 have a density of ≥1,800 targets/Km^2 and highlight that seven mass movement systems are moving with instability confined to the head (landslide 6 and 7) and the toe areas (landslides 11, 17, 18, 19 and 20) where LOS velocities reach 10 mm/yr in the descending geometry. A poor targets coverage characterises the landslides between Termini and Nerano but, based on geomorphological and ISBAS data, we can realistically assume that none or limited motion occurs here.

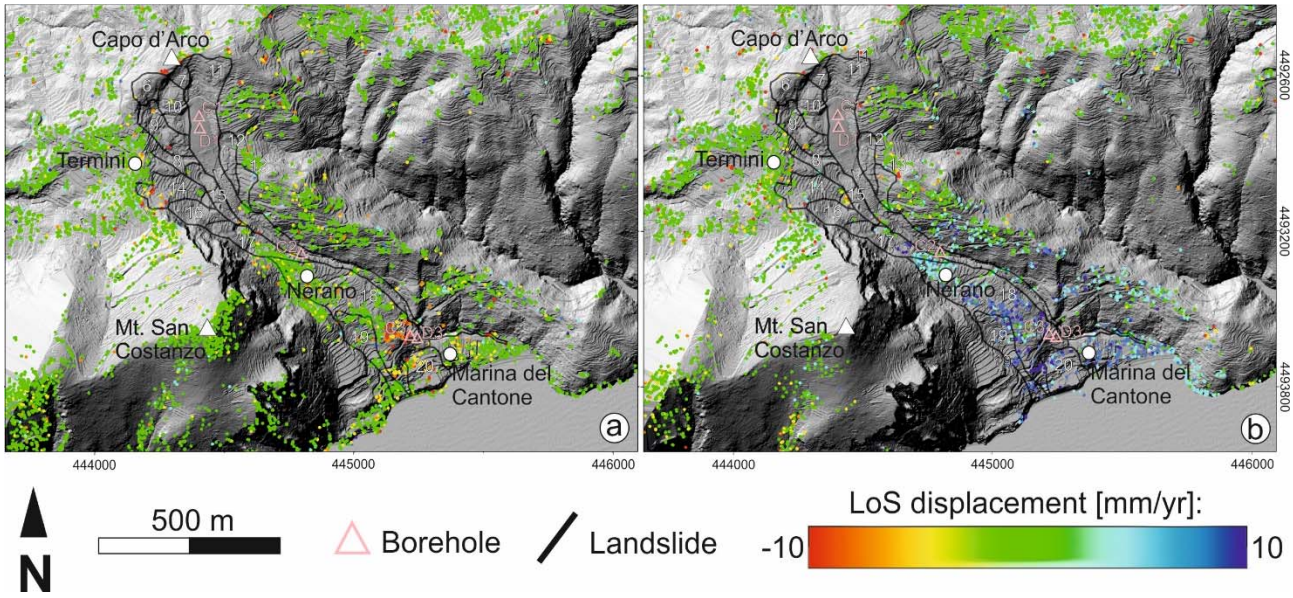

Fig. 9. *InSAR displacements along the LOS obtained from the CSK ascending (a) and CSK descending (b) data. Positive numbers correspond to motions towards the sensor, negative ones to motion away from the sensor along the LOS. Coordinate system: WGS 1984, UTM Zone 33N.*

Where CSK radar targets were sufficiently covering displacing masses (landslides 11, 17, 18, 19 and 20), the ascending and descending LOS displacements have been projected along horizontal and vertical directions after interpolation through the IDW method and application of Dalla Via et al. (2012) formula. The derived time series have been averaged in time, considering the closest satellite acquisitions, and in space, considering the same landslide body identified from field surveys, in order to be compared with the monthly rainfall record of the area available from the Massa Lubrense raingauge station, located ~3 km northwest of our study area.

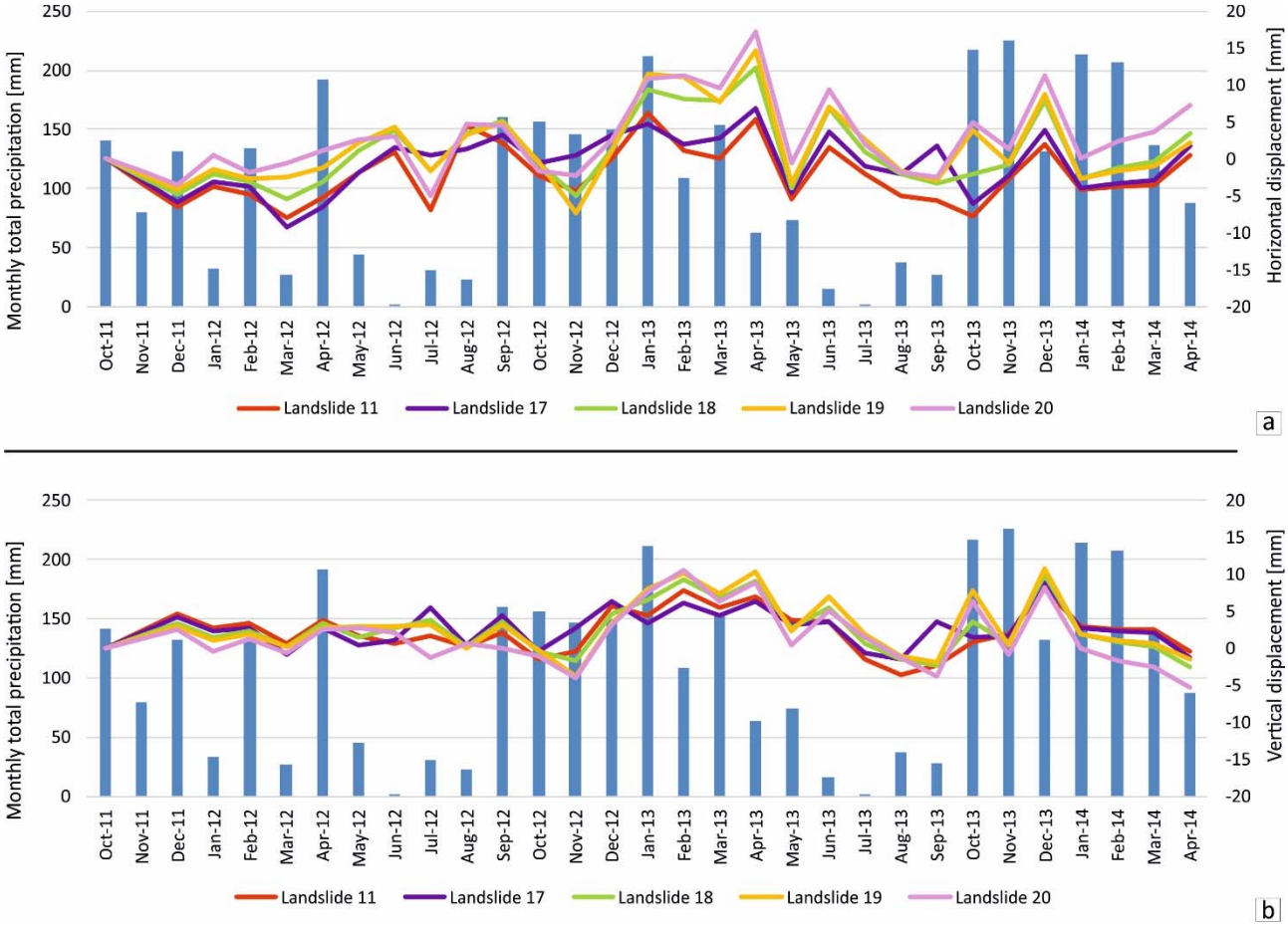

Fig. 10. *Average displacements for landslides 17, 18, 19 and 20 projected along the horizontal (a) and vertical (b) direction. Blue bars indicate monthly total precipitation.*

Following Bonì et al. (2018) classification method for the InSAR time series, the temporal analysis reveals that landslides move seasonally (non-linearly) with acceleration during Winter months and deceleration in Summer months and a time lag of 2-4 months with the precipitation peaks (Fig. 10). This temporal heterogeneity is more evident for the horizontal motion. While the geometry of the large mass events controls the development/reactivation of smaller rotational and complex landslides within the valley (see Section 4.2), InSAR time series analysis reveals that seasonal stress perturbations control the magnitude of the motion rates at a short temporal scale.

Finally, C1 and C3 inclinometers data have been used to validate the nearest PSP points available for the same time interval (Table 2) after the InSAR horizontal and vertical components of displacement have been spatially interpolated. The lack of a PSP in correspondence of each inclinometer might explain the tiny differences between the two measurements that overall agree and confirm the highest

444 deformation rates at the toe of landslide 18. The latter represents an unstable body where nearly 30m
445 of materials have been piled up collecting deposits transported within the whole Termini-Nerano
446 valley.
447
448 ***Table 2****. Comparison between inclinometer and interferometric data. For the borehole location, see Figure 9.*

Inclinometer	Period of acquisition (m/yyyy)	Inclinometer displacement (mm)	Inclinometer azimuth (°)	InSAR displacement (mm)	InSAR horizontal displacement (mm)
C1	*9/2012 – 2/2013*	*5.0*	*140 (SE)*	*1.5*	*3.9*
C3	*9/2012 – 2/2013*	*20.0*	*180 (S)*	*10.7*	*14.3*

449
450
451 *4.5 Landslide Hazard Mapping*
452 Fourteen environmental variables considered as predisposing factors have been selected to produce
453 H: slope angle, slope aspect, profile curvature, planform curvature, Topographic Wetness Index
454 (TWI), Topographic Position Index (TPI), InSAR horizontal velocity (according to the interpolation
455 shown in Section 4.4), elevation, distance to stream, distance to road, stream density, road density,
456 lithology and land-use. A more detailed description of these is given in Supplementary 2.
457 Apart from InSAR displacements, the selected environmental variables represent standard factors for
458 landslide hazard mapping (Van Westen et al., 2008).. To maintain the temporal consistency of all the
459 input datasets, only the interpolated horizontal InSAR data from CSK have been used (see Section
460 4.4) in combination with the LiDAR-derived geomorphological indicators and the outcropping layers
461 mapped during our field investigations. All the layers are raster (including the InSAR results after the
462 interpolation) that have been interpolated and brought to the same spatial resolution (10 m) and
463 extension. Considering the (i) assumption made for the volume calculation in Section 4.3, the vertical
464 differences from the original topography could not be used as training layer but for validation
465 purposes only, being limited to the landside areas.

Each stand-alone model (ANN, GBM and MaxEnt) was executed with 50 different combinations of training and testing of the data using the K-CV approach (Figs. 11a-c). Such a method allows to generate 150 different H scenarios with corresponding errors values and evaluation scores (Supplementary 1). In the ensemble procedure stand-alone models with a threshold > 0.7 for AUC and 0.6 for TSS only were selected. In this way, in the aforementioned procedure were chosen only the models with a good performance. The median of the probabilities of the three models has been chosen as the ensemble technique to obtain the final landslide susceptibility map, being the median less sensitive to outliers than the mean. The final ensemble map has an AUROC value of 0.96 and a TSS value of 0.82 (Fig. 11d).

The values of H, and later of E, V and R as well, have been grouped into four different classes to adhere to the Italian laws on hazard and risk assessment. The natural breaks method has been chosen to divide the distribution in these classes so to minimize the variance within each class and maximizing the variance between the classes (Fig. 11).

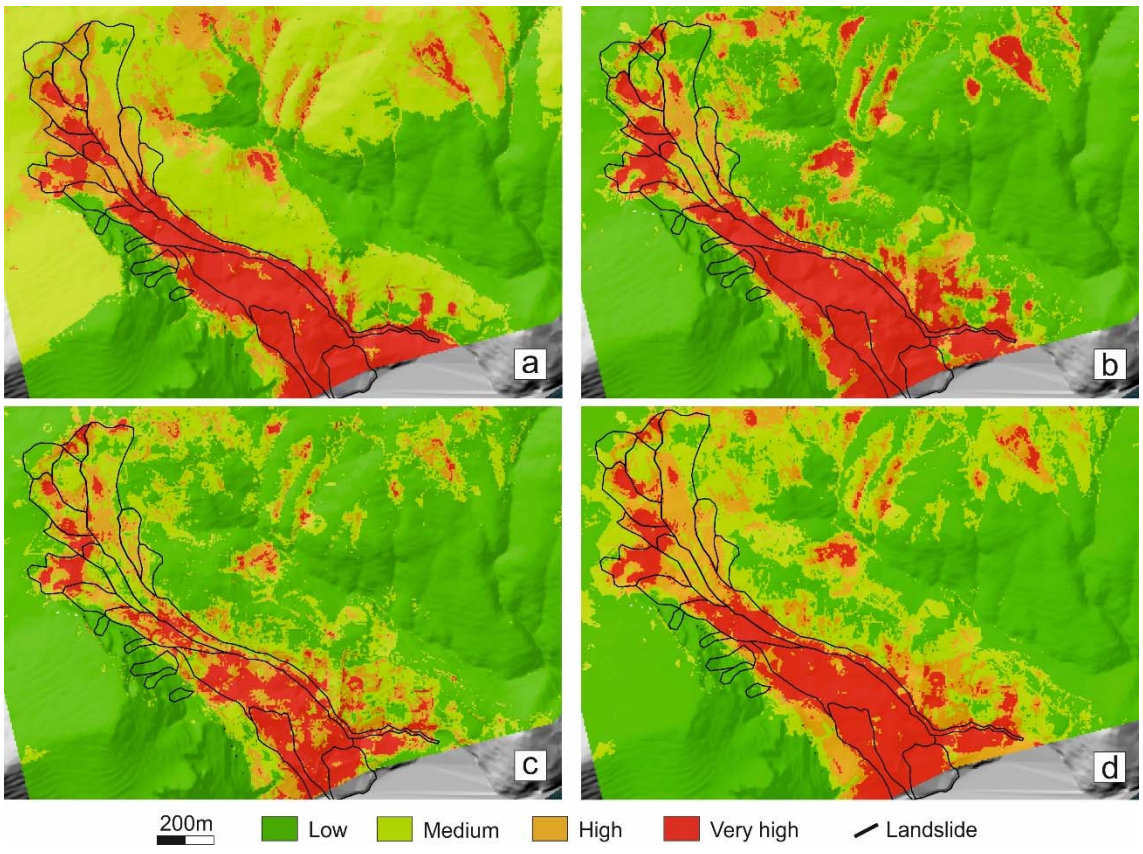

480 ***Fig. 11.*** *Median value of the hazard map from 50 ANN runs (a), from 50 GBM runs (b) and from 50 MaxEnt runs (c).*
481 *EM landslide hazard map considering median values from the 50 ANN, 50 GBM and 50 MaxEnt models (d).*
482

483 EM shows that the highest hazard is located on the northwestern sector at the toe of the landslide
484 system with only landslides 6, 10, 12, 13 and 15 presenting a low to medium risk. On the other hand,
485 whole landslide bodies (18, 19 and 20) show a very high hazard. Additional hazard is posed by the
486 bottom of the Mt. San Costanzo eastern slope. Score values, between 0 and 1, indicate how the factors
487 in EM contributed to H (Table 3). It has to be highlighted that we have not considered interactions
488 between variables so every factor has been examined independently. Scores close to 1 greatly affect
489 H while values close to 0 have no influence on the landslide hazard. Three main predisposing factors
490 emerge: horizontal displacement, slope aspect and the road density.

491 ***Table 3****. Scores of the fourteen variables used in the EM.*

Factor	Score	Factor	Score
Distance to road	0.042	Profile curvature	0.01
Distance to stream	0.008	Road density	0.136
Elevation	0.037	Slope angle	0.025
Lithology	0.03	Slope aspect	0.144
InSAR displacement	0.237	Stream density	0.055
Land-use	0.001	TPI	0.027
Planform curvature	0.029	TWI	0.009

492

493 InSAR displacement is the most influential factor, highlighting the importance of regularly
494 monitoring such type of landslides for building a reliable H. Consequently H tend to be higher where
495 velocities are the greater. The south facing aspect is an important factor especially if considered with
496 respect to the attitude of the TSF strata whose dip directions converge toward the Termini-Nerano
497 valley. Indeed, over the north facing slope just north of Capo d'Arco, no landslide is reported.
498 Road density is acknowledged to be a predisposing factor especially in the centre of Nerano, where
499 narrow scenic road snakes within the village, but not a triggering factor since there is no temporal
500 relationship between the road works and the occurrence of the landslide. Lithology is not a
501 predominant predisposing factor as the largest contrast in the mechanical and structural properties,
502 according to the borehole data (see Section 4.1), lies within the different landslide deposits developed

in the same unit, the TSF. Similarly, slope angle has a low influence on H since slow-moving landslides in SCFs can develop and move on low angle slopes (<10°), flat, or even slightly uphill terrains (Del Soldato et al., 2018).

4.6 Landslide Risk Mapping

The LRM has been combined with information on its potential impact which is expressed by E and V. The latter have been sampled by ISTAT over six different units (Fig. 12). These units do not correspond to administrative or geomorphological boundaries but follow the guidelines of Regulation (EC) no. 1059/2003 of the European Parliament on the establishment of territorial units that can be used for statistical analyses of population and buildings across Europe.

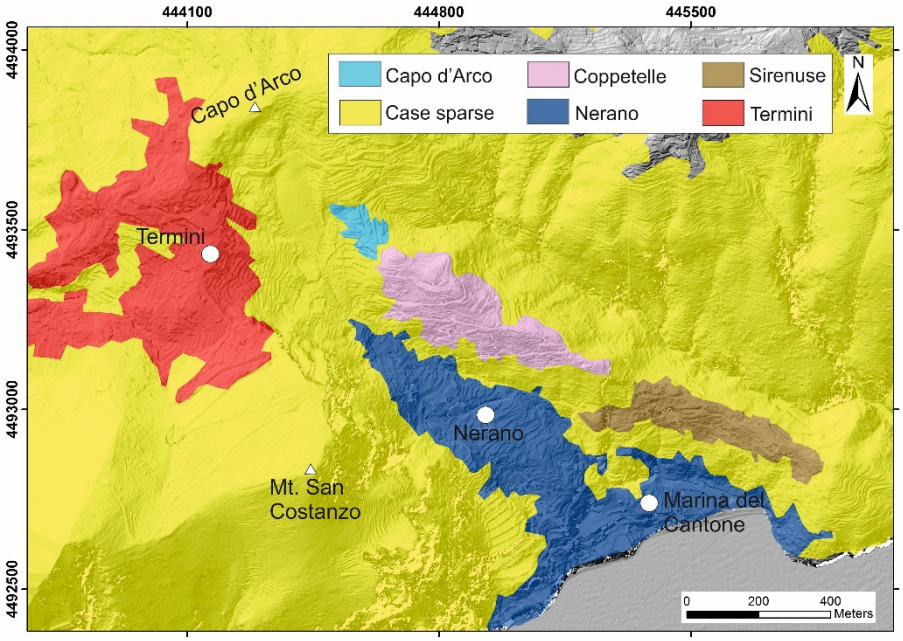

Fig. 12. *Territorial units defined by ISTAT for the Termini-Nerano area.*

Exposure information has considered information on the number of residents and building within the territorial unit.

Given the different size of each territorial unit, the density of buildings and population has been considered for E (Table 4). ISTAT does not provide information on the road network, so this information has been excluded, but it would spatially represent a minor component of the infrastructures here. About V, since most of the buildings are masonry and other types of buildings

(concrete, steel and wooden) represent <0.2% of the urban fabric, only the buildings age has been considered as a discriminant component for V.

***Table 4**. Main indicators used to extract element-at-risk and vulnerability inside the Termini-Nerano valley according to the ISTAT territorial units (see Figure 12).*

			density of buildings constructed in time			
Territorial Unit	**population/km2**	**buildings/km2**	**<1945**	**>1946 & <1970**	**>1971 & <2000**	**>2001**
Capo d'Arco	1,725	1,150	431	288	431	0
Case sparse	114	29	8	6	11	5
Coppetelle	2,331	802	246	182	310	64
Nerano	1,488	751	273	341	133	4
Sirenuse	688	398	15	260	122	0
Termini	2,255	754	278	172	260	44

V and E have then been normalized and summed to H according to the formula given in (1) and the LRM has been generated (Fig. 13a). R values range between 0 (low risk) and 1 (very high risk) and have been reclassified according to the natural breaks criterium. The low standard deviation (0.09) compared to the ranges of each class of R into a high precision for our map (Fig. 13b).

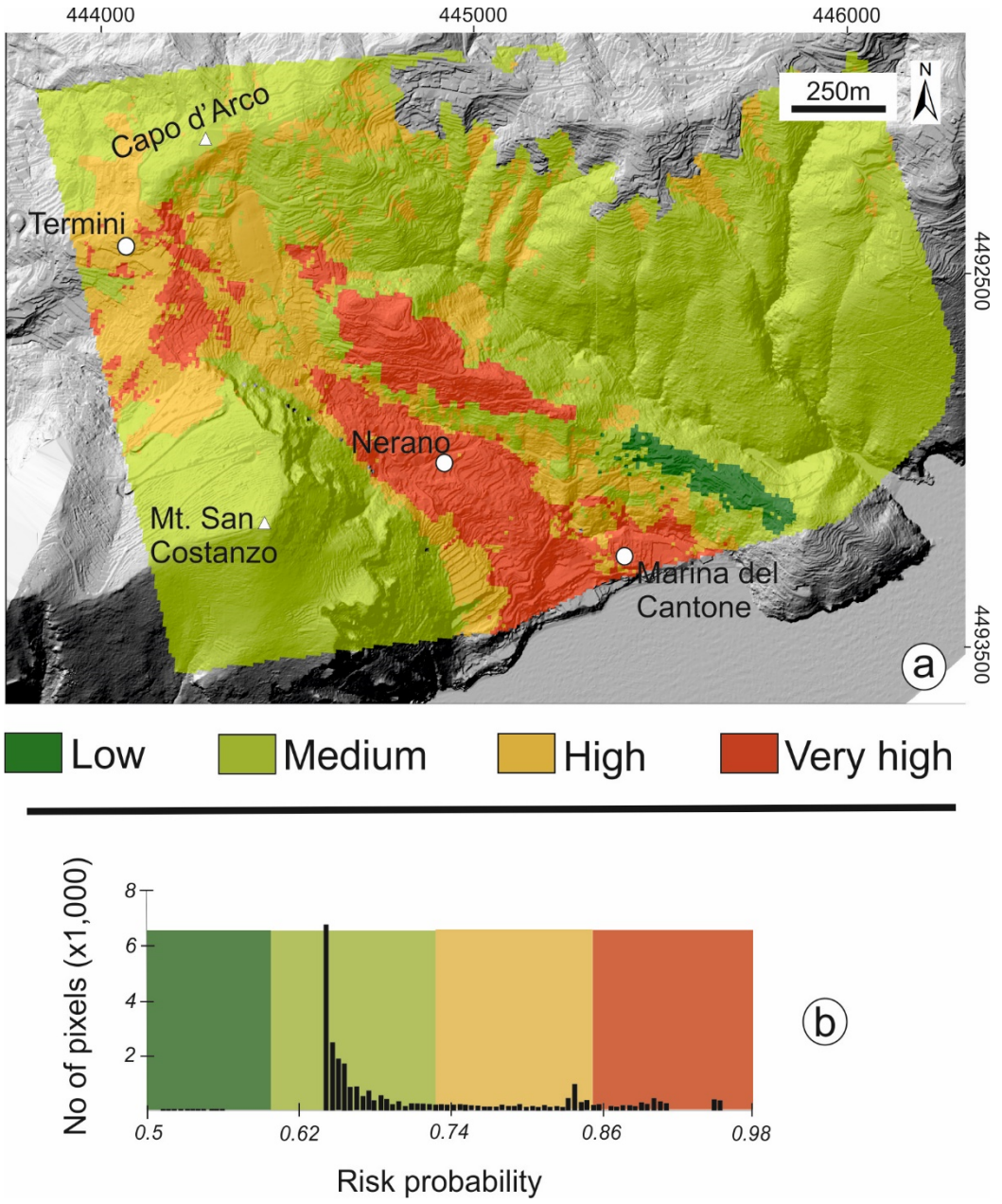

530

531 ***Fig. 13.*** *Landslide Risk Map for the Termini-Nerano valley (a) and corresponding histogram (b).*

532

533 According to the LRM, most of the valley is under medium and high risk with the highest risk located
534 south of Termini and in the bottom part of the valley, where most of the recorded damage has been
535 mapped (see Figure 5). The very high risk southeast of Termini and on the eastern side of the Termini-
536 Nerano valley is associated to the high population density and old building age while the very high
537 risk in Nerano is mainly due to H despite the lower population density (E) and relatively younger
538 buildings (V). In turn, the very high H in Nerano is mainly due to InSAR displacement. A medium

539 to high risk is instead characterising the top of the valley as result of the low density of population
540 and buildings in those territorial unit.
541
542
543 **5. Discussion**
544 The Termini-Nerano valley has been chosen as test area for developing a new methodology to assess
545 landslide risk due to the range of datasets available. The latter has allowed to build a multidisciplinary
546 approach which provides a holistic understanding of the landslide risk in the catchment where, in the
547 meantime, local population has lost the historical memory of the landslides activity (more than a
548 generation) and so underestimate the current risk.
549 In the studied area, geological and geomorphological observations have identified fifteen extremely-
550 slow-moving landslides, according to the Cruden and Varnes (1996) classification scheme, covering
551 a total area of 4.1×10^5 m^2.
552 Field mapping reveals that one of the most important controlling factors for landslides susceptibility
553 is the lithology given by the dip-slope attitude of the TSF layers and its role for the geometrical
554 distribution and evolution of the instabilities. Indeed, the valley evolution is characterised by large
555 and catastrophic movements, like the 1941 and 1963 with velocities up to m/h, who redistribute large
556 volumes of material from the TSF. Between these big events, however, the slope is continuously
557 reshaped by smaller instabilities that mainly redistribute the material within the toe area. We retrieved
558 the volume of each landslide deposit from the LiDAR-reconstructed topography and estimate a total
559 volume of ~1.484×10^6 m^3 for the whole landslides system. The net mass increase (0.016×10^6 m^3)
560 represents ~1% of the total volume calculation and can be attributed to: errors in the regression and
561 interpolation method, topographic reprofiling from anthropogenic activities and contamination of fall
562 deposits from Mt. San Costanzo. InSAR results prove the correlation between ground motion and
563 precipitation with seven mass movements that can be still considered active but with an intermittent

564 activity, a typical characteristic of landslides in heterogeneous terrains, such as the SCF, characterised
565 by a long activity history with continuous reactivations (Milillo et al., 2014).
566 A longer record and more dense groundwater observations are needed to fully understand the
567 hydrogeological conditions of the area such as the different response in groundwater rise observed
568 in D1 and D3.InSAR data confirms the correlation between rates of motion and precipitation. A
569 longer record of InSAR data, such as the inclusion of 7 years' worth of data from the Sentinel-1
570 constellation, would provide additional information to constraint the return period of the slope
571 instabilities. Despite several engineering drainage solutions have been erected in the head area during
572 the 1960s to mitigate the landslide hazard, InSAR displacements reveal that they have not been
573 effective in stabilizing the slope. The updated landslide inventory map, InSAR displacements, land
574 cover map and geomorphometric parameters have been used for the hazard assessment. Although
575 several MLAs methods have been explored for the spatial-temporal prediction of landslides (Thai
576 Pham et al., 2019), EM still represents a novelty and mainly limited to rapid or shallow landslides
577 (Carotenuto et al., 2017). In this work we have taken a step forward and used EM for assessing the
578 landslide hazard of slow-moving phenomena. Critical for the accuracy of EM is the selection of
579 training points and input layers (Micheletti et al., 2014). Ideally, training points are selected over
580 clearly identifiable landsliding areas, such a task can be relatively challenging in slow-moving
581 landslide which might not show signs of instabilities unless a detailed field survey is carries out.
582 Another important benefit of the landslides system in the Termini-Nerano Valley is that we could
583 chose training and validation pixels from different landslides within the same valley thus to avoid
584 unrealistic overestimations of prediction accuracy when training and validation points belong to the
585 instability. In our EM we include InSAR displacements among the input layers, being velocities the
586 only dynamic information needed to derive a hazard rather than a susceptibility map. The use of
587 InSAR as input for improving or refining susceptibility/hazard model is not rare (e.g., Carlà et al.,
588 2016; Ciampalini et al., 2016) but equivalently, InSAR can also be seen as a validation tool of such
589 models especially when data available is scarce. However, in this work we considered ground motion

590 as a predisposing factor, based on the idea that landslides in SCFs have a long reactivation history
591 and therefore catastrophic/sudden failures always affect sectors previously unstable. Whether is
592 training or validation, the uneven distribution of InSAR targets with a lower density over vegetated
593 areas is a critical aspect . In such case, interpolation methods can mask or amplify ground
594 displacements. . The advent of novel InSAR processing techniques, such as the Intermittent Small
595 Baseline Subset (ISBAS, Cigna and Sowter, 2017) or SqueeSAR (Ferretti et al., 2011), offer the
596 possibility of filling this gap by increasing the density of InSAR measurements.
597 Out of the fourteen layers used for the hazard map, ground displacements is the dominant one so,
598 even if they are considered slow-moving landslides, velocity still remains critical parameters that
599 need to be included and regularly updated for hazard and risk calculations as already acknowledge in
600 previous works (Casagli et al., 2016).
601 We used the vertical differences derived from the LiDAR DTM to validate the landslide hazard map.
602 The comparison shows that the areas with very high risk corresponds to areas with the vertical
603 differences are either highest (between Nerano and Marina del Cantone) or lowest (south of Termini).
604 Accumulation areas indeed are the fast-moving part within the valley with the old landslide deposits
605 that have historically supplied unstable materials for rapid events during the 20th century. On the other
606 hand, we interpreted the already depleted areas to be still unstable given the combination of the slope
607 aspect, slope angle and planform curvature for these exposed landforms.
608 Despite the highlighted limitations, we have a unique collection of data sufficient to improve the
609 current LRM for three reasons: updated information on the geometry and kinematic of the
610 instabilities, a combination of three MLAs for H and the different age of the buildings has been
611 considered for V.
612 Compared to the SAHD, our LRM define, overall, a more dangerous scenario where the area nearby
613 Nerano and Marina del Cantone from a low to medium level are now classified as a high-risk level
614 and the highest level of risk is now corresponding to areas south of Termini and on the eastern side
615 of the valley. Field surveys confirm damage to roads and walls within these sectors. The highest

difference with the SAHD LRM is over the eastward facing slope of Mt. San Costanzo because we did not account for the hazard associated to falls and topples affecting the Radiolitidae limestone Formation being it beyond the scope of this work. We have used a standard approach to evaluate R by providing the same weights for H, E and V. This, inevitably has penalised the amount of information within H which is a pixel-based layer compared to V and E that, on the other side, is a polygon-based census unit. Considering the amount of geological, geomorphological and kinematic conditioning factors which have been ingested in the risk assessment calculations, some of them with nonlinear distributions (e.g, InSAR data, E and V), single statistical or ML methods can easily bring to completely different risk scenarios. These standalone maps can show large discrepancies especially when are compared against each other, have to be updated or upscaled (Jacobs et al., 2020). On the other side, EM has enhanced the power prediction of individual classifiers while decreasing noise and over-fitting problems by combining different MLAs together.

6. Conclusions

Assessing landslide risk is one of the highest challenges in land management and is usually delegated to national institutions such as geological/environment surveys, civil protection agencies or the River Basin Authorities in the case of Italy (Solari et al., 2020). Better risk assessment would support the development of strategies towards disaster risk management and disaster risk reduction. As landslide activity is expected to grow worldwide as a result of a changing climate (Gariano and Guzzetti, 2016), the capacity to timely and properly predict landslide susceptibility is critical. The current study contributes to the advancement of landslide risk analyses. Indeed, an innovative methodology for producing LRMs, with the combination of InSAR and EM, has been developed and implemented over the Termin-Nerano landslides system where we could complement standard field surveys and geological investigations with different remote sensing data.

642 The exploitation of MLAs is still in its infancy, far away to become a standard practice to support
643 researchers, public entities, authorities and civil protection agencies which have the mandate to
644 generate landslides risk mapping. However, under the pressure of the latest remote sensing
645 technologies which provide regular and freely observations at continental scale, it has been already
646 recognised the importance of harmonised landslide hazard and risk map at continental scale following
647 the European landslide susceptibility map (Wilde et al., 2018). Such products will represent valuable
648 outcomes for focussing resources and implement medium to long term precautionary measures in
649 prevention, emergency and post-crisis mitigation phases. In particular, satellite platform and
650 downstreaming services are supplying geomorphological/kinematic data and information which has
651 been acknowledged to be the main obstacle for producing reliable landslide hazard and risk maps
652 from MLAs (Nsengiyumva and Valentino, 2020).
653 The use of the proposed ML-based landslide risk assessment method can be therefore particular
654 beneficial if dealing with large datasets at continental scale to be regularly updated considering that
655 slides, flows and complex movements (usually evolving as slow-moving landslides) represent more
656 than half of the 849,543 landslide events in Europe (Herrera et al., 2018). With this respect, the
657 Termini-Nerano valley represents a perfect case study given the amount of high-resolution data
658 available from remote sensing and ground-based techniques that have been used for developing,
659 performing and validating for the first time this innovative solution where InSAR and MLAs are
660 combined to produce a LRM.
661 Recent initiatives at continental scale work in favour of the replicability of our approach:
662 • InSAR datasets will be freely accessible at continental scale through the upcoming European
663 Ground Motion Service (Crosetto et al., 2020) based on Sentinel-1 satellite data. This service
664 will be of pivotal importance for landslide mapping activities at a national and regional scale.
665 • The MLAs used here are available for free across the most common statistics library of R-
666 Studio and Python for example. MLAs are able to account for and large training datasets and

667 EM, in particular, is a powerful tool which can account for different data-driven approaches
668 together to regularly update or upscale landslide hazard maps.
669 • Data on population and buildings, from which V and E can be calculated, are nowadays easily
670 accessible, homogenised and regularly collected at European level through the national
671 statistics offices and made available at any user.
672
673 Further research, however, is needed to further develop the presented ML-based methodology in order
674 to minimize subjectivity for selecting the different sources, resolution and mapping units associated
675 with the input datasets, usually determined by the available datasets, and to extend it to different
676 typologies of landslides.
677
678
679
680 **Acknowledgments**
681 Many thanks are due to Italian Ministry of Environment and Protection of Land and Sea who
682 supported the realization of the PST-A and to the European Space Agency, for the acquisition of the
683 ENVISAT and COSMO-SkyMed imagery. This research was partially funded by the University of
684 Naples Federico II and the Italian Compagnia di San Paolo Foundation (grant F.A.R.O. 2011) granted
685 to Dipartimento di Scienze della Terra, dell'Ambiente e delle Risorse. A. Novellino performed the
686 analysis during his PhD at the University of Naples and published with the permission of the
687 Executive Director of the British Geological Survey (BGS-NERC). C.U.G.RI (Consortium between
688 the Federico II University of Naples and the University of Salerno for the Prediction and Prevention
689 of Major Hazards) is gratefully acknowledged for supporting this research with hardware/software
690 facilities. The authors would like to acknowledge D. Boon and R. Ciurean from the British Geological
691 Survey for their valuable suggestions to improve the quality of the paper.
692

693

694

695

696 **References**

697 Alvarez, W., 1991. Tectonic evolution of the Corsica-Apennines-Alps region studied by the method of
698 successive approximations. Tectonics, 10(5), 936-947. https://doi.org/10.1029/91TC00232

699 Andrejev, K., Krušić, J., Đurić, U., Marjanović, M. and Abolmasov, B., 2017, May. Relative Landslide Risk
700 Assessment for the City of Valjevo. In Workshop on World Landslide Forum (pp. 525-533). Springer, Cham.

701 Arabameri, A., Pradhan, B., Lombardo, L., 2019. Comparative assessment using boosted regression trees,
702 binary logistic regression, frequency ratio and numerical risk factor for gully erosion susceptibility modelling.
703 CATENA, 183, 104223. https://doi.org/10.1016/j.catena.2019.104223

704 Araujo, M.B., Pearson, R.G., Thuiller, W., Erhard, M., 2005. Validation of species-climate impact models
705 under climate change. Global Change Biology 11(9), 1504–1513. https://doi.org/10.1111/j.1365-
706 2486.2005.01000.x

707 Aslan, G., Foumelis, M., Raucoules, D., De Michele, M., Bernardie, S. and Cakir, Z., 2020. Landslide Mapping
708 and Monitoring Using Persistent Scatterer Interferometry (PSI) Technique in the French Alps. Remote
709 Sensing, 12(8), p.1305. https://doi.org/10.3390/rs12081305

710 Bartolini, S., Cappello, A., Martí, J., Del Negro, C., 2013. QVAST: a new Quantum GIS plugin for estimating
711 volcanic susceptibility. Nat. Hazards Earth Syst. Sci, 13(11), 3031-3042. https://doi.org/10.5194/nhess-13-
712 3031-2013

713 Bonì, R., Bosino, A., Meisina, C., Novellino, A., Bateson, L., McCormack, H., 2018. A methodology to detect
714 and characterize uplift phenomena in urban areas using Sentinel-1 data. Remote Sensing, 10(4), p.607.
715 https://doi.org/10.3390/rs10040607

716 Brugner, W., Valdinucci, A., 1973. Landslide classification scheme and correpsonding examples. Bollettino
717 del Servizio Geologico d'Italia, 73-110. [in Italian]

718 Canuti, P., Dramis, F., Esu, F., 1992. Stability conditions over urbanised slope: principles and general
719 guidelines for public institutions. CNR-GNDCI, 544, 100 pp. [in Italian]

720 Carlà, T., Raspini, F., Intrieri, E. and Casagli, N., 2016. A simple method to help determine landslide
721 susceptibility from spaceborne InSAR data: the Montescaglioso case study. Environmental Earth Sciences,
722 75(24), pp.1-12. https://doi.org/10.1007/s12665-016-6308-8

723 Carotenuto, F., Angrisani, A.C., Bakthiari, A., Carratù, M.T., Di Martire, D., Finicelli, G.F., et al., 2017. A
724 new statistical approach for landslide susceptibility assessment in the urban area of Napoli (Italy). In:
725 Workshop on World Landslide Forum. Springer, Cham, pp 881–889

726 Casagli, N., Cigna, F., Bianchini, S., Hölbling, D., Füreder, P., Righini, G., et al., 2016. Landslide mapping
727 and monitoring by using radar and optical remote sensing: Examples from the EC-FP7 project SAFER. Remote
728 sensing applications: society and environment, 4, pp.92-108. https://doi.org/10.1016/j.rsase.2016.07.001

729 Cesarano, M., Bish, D.L., Cappelletti, P., Cavalcante, F., Belviso, C., Fiore, S., 2018. Quantitative mineralogy
730 of clay-rich siliciclastic landslide terrain of the Sorrento Peninsula, Italy, using a combined XRPD and XRF
731 approach. Clays Clay Min, 66 (4), 353-369. https://doi.org/10.1346/CCMN.2018.064108

732 Chang, K. J., Chan, Y. C., Chen, R. F., Hsieh, Y. C., 2018. Geomorphological evolution of landslides near an
733 active normal fault in northern Taiwan, as revealed by lidar and unmanned aircraft system data. Nat. Hazards
734 Earth Syst. Sci, 18, 709-727. https://doi.org/10.5194/nhess-18-709-2018

735 Chen, W., Pourghasemi, H. R., Kornejady, A., Zhang, N., 2017. Landslide spatial modeling: Introducing new
736 ensembles of ANN, MaxEnt, and SVM machine learning techniques. Geoderma. 305, 314-327.
737 https://doi.org/10.1016/j.geoderma.2017.06.020

738 Ciampalini, A., Raspini, F., Lagomarsino, D., Catani, F. and Casagli, N., 2016. Landslide susceptibility map
739 refinement using PSInSAR data. Remote Sensing of Environment, 184, pp.302-315.
740 https://doi.org/10.1016/j.rse.2016.07.018

741 Cigna, F., Sowter, A., 2017. The relationship between intermittent coherence and precision of ISBAS InSAR
742 ground motion velocities: ERS-1/2 case studies in the UK. Remote sensing of environment, 202, pp.177-198.
743 https://doi.org/10.1016/j.rse.2017.05.016

744 Confuorto, P., Di Martire, D., Centolanza, G., Iglesias, R., Mallorqui, J.J., Novellino, A., et al., 2017. Post-
745 failure evolution analysis of a rainfall-triggered landslide by multi-temporal interferometry SAR approaches
746 integrated with geotechnical analysis, Remote Sensing of Environment. 188, 51-72.
747 https://dx.doi.org/10.1016/j.rse.2016.11.002

748 Costantini, M., Falco, S., Malvarosa, F., Minati, F., Trillo, F., Vecchioli, F., 2014. Persistent scatterer pair
749 interferometry: approach and application to COSMO-SkyMed SAR data. IEEE J. Sel. Top. Appl. Earth Obs.
750 Remote Sens. 7 (7), 2869–2879. https://dx.doi.org/10.1109/JSTARS.2014.2343915

751 Costantini, M., Ferretti, A., Minati, F., Falco, S., Trillo, F., Colombo, D., et al., 2017. Analysis of surface
752 deformations over the whole Italian territory by interferometric processing of ERS, Envisat and COSMO-
753 SkyMed radar data. Remote Sens Environ. 202, 250-275. https://doi.org/10.1016/j.rse.2017.07.017G

754 Cotecchia, V., Melidoro, G. 1966. Geological observation of the Termini-Nerano landslide. Geol Appl Idrogol,
755 1, 93-122. [in Italian]

756 Crosetto, M., Solari, L., Mróz, M., Balasis-Levinsen, J., Casagli, N., Frei, M., et al., 2020. The Evolution of
757 Wide-Area DInSAR: From Regional and National Services to the European Ground Motion Service. Remote
758 Sensing, 12(12), p.2043. https://doi.org/10.3390/rs12122043

759 Cruden D.M., Varnes D.J., 1996. Landslide types and processes. In: Turner AK, Schuster RL (eds) Landslides
760 investigation and mitigation. Transportation research board, US National Research Council. Special Report
761 247, Washington, DC, Chapter 3, 36–75.

762 D'Argenio, B., Ferreri, V., & Amodio, S., 2011. Eustatic cycles and tectonics in the Cretaceous shallow Tethys,
763 Central-Southern Apennines. Italian Journal of Geosciences, 130(1), 119-127.

764 D'Elia, B., Picarelli, L., Leroueil, S., Vaunat, J., 1998. Geotechnical characterisation of slope movements in
765 structurally complex clay soils and stiff jointed clays. Rivista Italiana di Geotecnica 32(3), 5-47. [in Italian]

766 Dalla Via, G., Crosetto, M., Crippa, B., 2012. Resolving vertical and east-west horizontal motion from
767 differential interferometric synthetic aperture radar: The L'Aquila earthquake. Journal of geophysical research:
768 solid earth, 117(B2). https://doi.org/10.1029/2011JB008689

769 Del Soldato M., Riquelme A., Bianchini S., Tomàs R., Di Martire D., de Vita P., et al., 2018. Multisource data
770 integration to investigate one century of evolution for the Agnone landslide (Molise, southern Italy).
771 Landslides, 15(11), 2113-2128. https://doi.org/10.1007/s10346-018-1015-z

772 De Riso, R., Di Nocera, S., Pescatore, T., 2004. Special project for the study of unstable towns of the
773 Campania Region - SCAI project , 1, 258-263. Napoli, 2004. [in Italian]

774 Di Martire, D., Tessitore, S., Brancato, D., Ciminelli, M.G., Costabile, S., Costantini, M., et al., 2016.
775 Landslide detection integrated system (LaDIS) based on in-situ and satellite SAR interferometry
776 measurements. Catena, 137, 406-421. https://doi.org/10.1016/j.catena.2015.10.002

777 Di Martire, D.,Paci, M., Confuorto, P., Costabile, S., Guastaferro, S., Verta, A., et al., 2017. A nation-wide
778 system for landslide mapping and risk management in Italy: The second Not-ordinary Plan of Environmental
779 Remote Sensing. Int J Appl Earth Obs Geoinf. 36, 143-157. https://doi.org/10.1016/j.jag.2017.07.018

780 Di Napoli, M., Carotenuto, F., Cevasco, A., Confuorto, P., Di Martire, D., Firpo, M., et al., 2020. Machine
781 learning ensemble modelling as a tool to improve landslide susceptibility mapping reliability. Landslides, 1-
782 18. https://doi.org/10.1007/s10346-020-01392-9

783 Dou, J., Yamagishi, H., Pourghasemi, H.R., Yunus, A.P., Song, X., Xu, Y., Zhu, Z., 2015. An integrated
784 artificial neural network model for the landslide susceptibility assessment of Osado Island, Japan. Natural
785 Hazards, 78(3), pp.1749-1776. https://doi.org/10.1007/s11069-015-1799-2

786 Elith, J., Graham, C.H., Anderson, R.P., Dudík, M., Ferrier, S., Guisan, A., et al., 2006. Novel methods
787 improve prediction of species' distributions from occurrence data. Ecography 29(2):129–151.
788 https://doi.org/10.1111/j.2006.0906-7590.04596.x

789 Esu, F., 1977. Behaviour of slopes in structurally complex formations. Proceedings of the "International
790 Symposium on the geotechnics of Structurally Complex Formations", Capri: 292–304.

791 Fell, R., Corominas, J., Bonnard, C., Cascini, L., Leroi, E., Savage, W.Z., 2008. Guidelines for landslide
792 susceptibility, hazard and risk zoning for land-use planning. Engineering Geology, 102(3-4), 99-111.
793 https://doi.org/10.1016/j.enggeo.2008.03.022

794 Ferretti, A., Fumagalli, A., Novali, F., Prati, C., Rocca, F., Rucci, A., 2011. A new algorithm for processing
795 interferometric data-stacks: SqueeSAR. IEEE transactions on geoscience and remote sensing, 49(9), pp.3460-
796 3470. https:// 10.1109/TGRS.2011.2124465

797 Froude, M. J., Petley, D. N.: Global fatal landslide occurrence from 2004 to 2016, 2018. Nat. Hazards Earth
798 Syst. Sci., 18, 2161-2181. https://doi.org/10.5194/nhess-18-2161-2018

799 Gariano, S.L., Guzzetti, F., 2016. Landslides in a changing climate. Earth-Science Reviews, 162, pp.227-252.
800 https://doi.org/10.1016/j.earscirev.2016.08.011

801 Handwerger, A.L., Huang, M., Fielding, E.J., Booth A.M., Bürgmann, R., 2019.A shift from drought to
802 extreme rainfall drives a stable landslide to catastrophic failure. Sci Rep 9, 1569.
803 https://doi.org/10.1038/s41598-018-38300-0

804 Herrera, G., Mateos, R.M., García-Davalillo, J.C., Grandjean, G., Poyiadji, E., Maftei, R., et al., 2018.
805 Landslide databases in the Geological Surveys of Europe. Landslides, 15(2), pp.359-379.
806 https://doi.org/10.1007/s10346-017-0902-z

807 Hu, X., Bürgmann, R., Schulz, W.H., Fielding, E.J., 2020. Four-dimensional surface motions of the
808 Slumgullion landslide and quantification of hydrometeorological forcing. Nat Commun 11, 2792.
809 https://doi.org/10.1038/s41467-020-16617-7

810 Huang, F., Cao, Z., Guo, J., Jiang, S.H., Li, S., Guo, Z., 2020. Comparisons of heuristic, general statistical and
811 machine learning models for landslide susceptibility prediction and mapping. CATENA, 191, p.104580.
812 https://doi.org/10.1016/j.catena.2020.104580

813 Hungr, O., Leroueil, S., Picarelli, L., 2014. The Varnes classification of landslide types, an update. Landslides.
814 11(2), 167-194. https://dx.doi.org/10.1007/s10346-013-0436-y

815 Iannace, A., Capuano, M., Galluccio, L., 2011. "Dolomites and dolomites" in Mesozoic platform carbonates
816 of the Southern Apennines: geometric distribution, petrography and geochemistry. Palaeogeography,
817 Palaeoclimatology, Palaeoecology. 310, 324–339. https://doi.org/10.1016/j.palaeo.2011.07.025

818 ISPRA, 2015. Sheet index for Italian 1:50,000 geological series, sheet 466 "Sorrento".
819 http://www.isprambiente.gov.it/Media/carg/note_illustrative/466_485_Sorrento_Termini.pdf [in Italian]

820 ISPRA, 2018. Hydrogeological instability in Italy: hazard and risk indicators. Report 2018. [in Italian]

821 ISTAT, 2011. Population Housing Census. Available at http://dati-
822 censimentopopolazione.istat.it/Index.aspx?lang=en (accessed on 26/5/2020)

823 Jacobs, L., Kervyn, M., Reichenbach, P., Rossi, M., Marchesini, I., Alvioli, M., et al., 2020. Regional
824 susceptibility assessments with heterogeneous landslide information: Slope unit-vs. pixel-based approach.
825 Geomorphology, 356, p.107084. https://doi.org/10.1016/j.geomorph.2020.107084

826 Kim, H.G., Lee, D.K., Park, C., Ahn, Y., Kil, S-H., Sung S., et al., 2018 Estimating landslide susceptibility
827 areas considering the uncertainty inherent in modeling methods. Stoch Env Res Risk A 32:2987–3019.
828 https://doi.org/10.1007/s00477-018-1609-y

829 Lacroix, P., Handwerger, A.L., Bièvre, G., 2020. Life and death of slow-moving landslides. Nat Rev Earth
830 Environ 1, 404-419. https://doi.org/10.1038/s43017-020-0072-8

831 Micheletti, N., Foresti, L., Robert, S., Leuenberger, M., Pedrazzini, A., Jaboyedoff, M. and Kanevski, M.,
832 2014. Machine learning feature selection methods for landslide susceptibility mapping. Mathematical
833 geosciences, 46(1), pp.33-57. https://doi.org/10.1007/s11004-013-9511-0

834 Milillo, P., Fielding, E. J., Shulz, W. H., Delbridge, B., Burgmann, R., 2014. COSMO-SkyMed spotlight
835 interferometry over rural areas: The Slumgullion landslide in Colorado, USA. IEEE Journal of Selected Topics
836 in Applied Earth Observations and Remote Sensing, 7(7), 2919-2926.
837 https://doi.org/10.1109/JSTARS.2014.2345664

838 Mutti, E., Bernoulli, D., Ricci Lucchi, F., Tinterri, R., 2009, Turbidites and turbidity currents from
839 Alpine 'flysch' to the exploration of continental margins. Sedimentology, 56, 267–318.
840 https://doi.org/10.1111/j.1365-3091.2008.01019.x
841

842 Novellino, A., Cigna, F., Sowter, A., Syafiudin, M.F., Di Martire, D., Ramondini, M., et al., 2015. Intermittent
843 small baseline subset (ISBAS) InSAR analysis to monitor landslides in Costa della Gaveta, Southern Italy.
844 IEEE International Geoscience and Remote Sensing Symposium, IGARSS 2015; Milan; Italy.
845 https://doi.org/10.1109/IGARSS.2015.7326584

846 Novellino, A., Cigna, F., Sowter, A., Ramondini, M., Calcaterra, D., 2017a. Exploitation of the Intermittent
847 SBAS (ISBAS) algorithm with COSMO-SkyMed data for landslide inventory mapping in north-western
848 Sicily, Italy. Geomorphology. 280, 153-166. https://dx.doi.org/10.1016/j.geomorph.2016.12.009

849 Novellino, A., Cigna, F., Brahmi, M., Sowter, A., Bateson, L., Marsh, S., 2017b. Assessing the feasibility of
850 a national InSAR ground deformation map of Great Britain with Sentinel-1. Geosciences, 7(2), p.19.
851 https://doi.org/10.3390/geosciences7020019

852 Nsengiyumva, J.B. and Valentino, R., 2020. Predicting landslide susceptibility and risks using GIS-based
853 machine learning simulations, case of upper Nyabarongo catchment. Geomatics, Natural Hazards and Risk,
854 11(1), pp.1250-1277. https://doi.org/10.1080/19475705.2020.1785555

855 Pappalardo G., Mineo S., Angrisani A.C., Di Martire D., Calcaterra D., 2018. Combining field data with
856 infrared thermography and DInSAR surveys to evaluate the activity of landslides: the case study of Randazzo
857 Landslide (NE Sicily). Landslides, 15(11), 2173-2193. https://doi.org/10.1007/s10346-018-1026-9

858 SAHD, 2011a. Landslide Inventory Map. Available at archive for the SAHD maps (accessed on 24/10/2018).
859 [in Italian]

860 SAHD, 2011b. Landslide Risk Map. Available at archive for the SAHD maps (accessed on 10/5/2020). [in
861 Italian]

862 SAHD, 2011c. Geomorphological Map. Available at archive for the SAHD maps (accessed on 12/5/2020). [in
863 Italian]

864 Salvati, P., Bianchi, C., Rossi, M., Guzzetti, F., 2010. Societal landslide and flood risk in Italy. Nat. Hazards
865 Earth Syst. Sci. 10, 465–483. https://dx.doi.org/10.5194/nhess-10-465-2010

866 Sepe, C., Confuorto, P., Angrisani, A.C., Di Martire, D., Di Napoli, M., Calcaterra, D., 2019. Application of
867 statistical approach to landslide susceptibility map generation in urban settings. In Proc IAEG/AEG Annu
868 Meeting Proc. Springer, Cham, San Francisco, vol. 1, pp 155–162.

869 Solari, L., Del Soldato, M., Raspini, F., Barra, A., Bianchini, S., Confuorto, P., Casagli, N., Crosetto, M., 2020.
870 Review of satellite interferometry for landslide detection in Italy. Remote Sensing, 12(8), p.1351.
871 https://doi.org/10.3390/rs12081351

872 Thai Pham, B., Shirzadi, A., Shahabi, H., Omidvar, E., Singh, S.K., Sahana, M., et al., 2019. Landslide
873 susceptibility assessment by novel hybrid machine learning algorithms. Sustainability, 11(16), p.4386.
874 https://doi.org/10.3390/su11164386

875 Thuiller, W., Lafourcade, B., Engler, R., Araújo, M.B., 2009. BIOMOD - a platform for ensemble forecasting
876 of species distributions. Ecography 32, 369–373. https://doi.org/10.1111/j.1600-0587.2008.05742.x

877 Van Westen, C.J., Castellanos, E., Kuriakose, S.L., 2008. Spatial data for landslide susceptibility, hazard, and
878 vulnerability assessment: an overview. Engineering geology, 102(3-4), pp.112-131.
879 https://doi.org/10.1016/j.enggeo.2008.03.010

Vinci, F., Iannace, A., Parente, M., Pirmez, C., Torrieri, S., Giorgioni, M., 2017. Early dolomitization in the Lower Cretaceous shallow-water carbonates of Southern Apennines (Italy): Clues about palaeoclimatic fluctuations in western Tethys. Sedimentary Geology. 362, 17-36. https://doi.org/10.1016/j.sedgeo.2017.10.007

Vitale, S., Tramparulo, F. D. A., Ciarcia, S., Amore, F. O., Prinzi, E. P., Laiena, F., 2017. The northward tectonic transport in the southern Apennines: examples from the Capri Island and western Sorrento Peninsula (Italy). International Journal of Earth Sciences. 106(1), 97-113. https://doi.org/10.1007/s00531-016-1300-9

Wilde, M., Günther, A., Reichenbach, P., Malet, J.P., Hervás, J., 2018. Pan-European landslide susceptibility mapping: ELSUS Version 2. Journal of maps, 14(2), pp.97-104. https://doi.org/10.1080/17445647.2018.1432511